THE HONG KONG
POLYTECHNIC UNIVERSITY
香港理工大學
Pao Yue-kong Library
包玉剛圖書館

Copyright Undertaking

This thesis is protected by copyright, with all rights reserved.

By reading and using the thesis, the reader understands and agrees to the following terms:

1. The reader will abide by the rules and legal ordinances governing copyright regarding the use of the thesis.
2. The reader will use the thesis for the purpose of research or private study only and not for distribution or further reproduction or any other purpose.
3. The reader agrees to indemnify and hold the University harmless from and against any loss, damage, cost, liability or expenses arising from copyright infringement or unauthorized usage.

If you have reasons to believe that any materials in this thesis are deemed not suitable to be distributed in this form, or a copyright owner having difficulty with the material being included in our database, please contact lbsys@polyu.edu.hk providing details. The Library will look into your claim and consider taking remedial action upon receipt of the written requests.

Pao Yue-kong Library, The Hong Kong Polytechnic University, Hung Hom, Kowloon, Hong Kong

http://www.lib.polyu.edu.hk

Time-Domain Prediction of Acoustics in Domains with Realistic Boundaries

by

Wai Sun SHUM

Department of Mechanical Engineering

The Hong Kong Polytechnic University

A thesis submitted in partial fulfillment of the requirements for the degree of

Master of Philosophy (1997-1999)

Pao Yue-Kong Library
PolyU • Hong Kong

Acknowledgment

My thanks go to the invaluable suggestions and the research opportunity from my advisors Prof. K.-Y. Fung, Prof. R.M.C. So and Dr. K.M. Li. Their help to me in the past two years had been a fantastic and an enjoyable learning experience. For Prof. Y.S. Wong, Prof. Grafton W.H. Hui and Prof. K.-Y. Fung, their presence as the examiners of the thesis oral examination is greatly appreciated. Prof. Arthur F.T. Mak had ensured the legibility of the thesis. Throughout this thesis, Prof. K.-Y. Fung had helped me to formulate the time-domain impedance boundary condition, the piston initial boundary value problem, and provided many useful algorithmic components for computation. Dr. K.M. Li guided me through the solution of an outdoor sound propagation problem. Prof. K.-Y. Fung and Prof. Grafton W.H. Hui had made indispensable comments on the writing of the thesis. The research was supported by the RPGC funding of the Hong Kong Polytechnic University.

Abstract

The validity of the recently proposed time-domain impedance boundary condition is explored. The one-dimensional piston in an impedance tube problem is formulated and attempted using the classical Laplace transform to compare with a recently developed time-domain method. It will be shown that the classical frequency-domain method does not lead to uniformly convergent analytic solutions in one-dimension, but to finite series approximations, which resemble the long time stable and accurate numerical solutions. The time-domain solution with time-domain impedance boundary condition is then compared with the frequency-domain solution of harmonic point sources near an impedance plane in two dimensions, which establishes the agreement between time-domain and frequency-domain approaches at discrete frequencies. Solutions for noise abatement with mixed impedance grounds using different mixed impedance models and Boundary Element Method (BEM) numerical scheme are compared with those using the time-domain approach. Applications and further extensions of the time-domain approach to problems in acoustics will be addressed.

CONTENTS

NOMENCLATURE

β acoustic admittance (= 1/Z).

c sound speed in air (= 340m/s).

$erfc(.)$ complementary error function with complex argument.

$F(p_e)$ boundary loss factor with p_e dependence.

h_r receiver height.

h_s source height.

k wave number of a wave (= ω/c).

υ Courant-Federick-Lewis (CFL) condition.

ω circular frequencies of an acoustic wave.

Ω single frequency component of a wave.

p total (direct + reflected) acoustic wave sound pressure level.

$\hat{p}$ Fourier component of sound pressure level p.

p_d direct wave sound pressure level.

p_t total (direct + reflected) acoustic wave sound pressure level.

p_e numerical distance.

ϕ acoustic potential.

$\hat{\phi}$ Fourier component of the acoustic potential ϕ.

Q spherical wave reflection coefficient.

r horizontal separation distance.

$R_0(\omega)$ resistance of an impedance $Z(\omega)$ with ω dependence.

$R(\theta)$ plane wave reflection coefficient with θ dependence.

R_1 direct wave path from the source to the receiver.

R_2 reflected wave path from the image source to the receiver.

θ angle of incidence measured from the incident wave to the normal of the surface.

u perturbed acoustic velocity in the x-direction.

u^+ $= u + p$.

$\hat{u}^+$ Fourier component of u^+.

v perturbed acoustic velocity in the y-direction.

v^+ $= v + p$.

$\hat{v}^+$ Fourier component of v^+.

w perturbed acoustic velocity in the z-direction.

w^+ $= w + p$.

$\hat{w}^+$ Fourier component of w^+.

$W(t)$ time-domain reflection coefficient.

$\hat{W}(\omega)$ frequency-domain reflection coefficient.

$X_0(\omega)$ reactance of an impedance $Z(\omega)$ with ω dependence.

$Z(\omega)$ specific acoustic impedance ($= R_0(\omega) + iX_0(\omega)$) with ω dependence.

Chapter 1 Introduction

1.1 Impedance Boundary Condition in Acoustics

The sound field of a sound source and its reflections from a soft boundary has been viewed as the superposition of the direct waves from the source with the reflected waves from the image source. The mathematical method for this solution is known as the method of superposition or the method of images. Due to the complexity of the reflecting surface, the amplitude and the phase angle of the reflected wave will be changed relative to the incident wave. Such changes of amplitude and phase angle can be mathematically related to a complex quantity. This complex quantity is frequency and incident angle dependent, which represents the acoustical properties of the reflecting surface. In addition, the reflected sound field from a material surface depends on the location of the source relative to the surface and the acoustical properties of the reflecting surface. These acoustical properties can be characterized by the acoustic impedance Z, which is defined as the ratio of the sound pressure level to the normal fluid velocity at the material surface. In mechanics, the ratio of force amplitude to velocity amplitude is referred as an impedance.[1] The concept of impedance, something impeding on motion, was first introduced to electric circuit theory as the ratio of voltage amplitude to current amplitude by Heaviside in the late nineteenth century.[1] Webster introduced impedance into acoustics in 1914 and independently by Kennelly and Kurokawa in 1921.[1] When the material has a high refractive index, the speed of the wave traveling in the material is much less than the speed of sound in air. In other words the refracted sound wave is strongly bent towards the normal to the surface.[2] Hence the surface is considered to be locally reacting. This means that Z depends only on the frequencies of the incident wave, or $Z = Z(\omega)$, where ω is the circular frequency of the wave. This happens when the

material has a high flow resistivity. For material with low flow resistivity, the acoustic impedance becomes dependent on the angle of incidence θ, which is measured from the incident wave toward the normal of a surface. Therefore, $Z = Z(\omega,\theta)$, in such a circumstance, the surface is described as non-locally reacting, externally reacting, extended reaction, or bulk reaction.[2]

1.2 Other Boundary Conditions

Apart from surfaces with uniform impedance treatment, there are also many other different boundary conditions. The wall of a building is an example of the rigid boundary if it reflects sound waves totally. In some cases, the walls inside a room are composed of different materials, such as glass windowpanes as vibrating panels on a wall, soft foam ceilings for heat insulation, and decorative picture hung on the wall as protrusion. This kind of wall is considered as a mixed impedance boundary. A train running on a track, or an automobile cruising on a freeway, is an example of sound reflection from a moving source over a stationary boundary. Practical acoustic surfaces are not flat in shape. A column inside a room is a curved convex hard boundary. Sound absorbing materials with corrugated surfaces could be lined inside an auditorium, a lecture theater or a music room. With human beings, furniture and pets inside a room, the prediction of sound reflection from the irregular boundaries becomes much more complicated.

1.3 Experimental Literature Review

There are many experimental methods to determine the specific acoustic impedance. Mellert et al. approximated impedance values from the measured spherical wave reflection coefficient.[3] Cramond and Don simplified the theory by ignoring the

surface wave term when computing the impedance.[4,5] Acoustic sound pressure level can be found if the admittance β is known and vice versa. In fact, Cramond and Don[4,5] used the Weyl Van der Pol formula[11,12] to compute the acoustic impedance. The Weyl Van der Pol formula has the following expression

$$\phi \cong \frac{\exp(ikR_1)}{4\pi R_1} + Q\frac{\exp(ikR_2)}{4\pi R_2}, \tag{1.1a}$$

$$Q = R(\theta) + (1 - R(\theta))F(p_e), \tag{1.1b}$$

$$R(\theta) = \frac{\cos(\theta) - \beta}{\cos(\theta) + \beta}, \tag{1.1c}$$

$$F(p_e) = 1 + i\sqrt{\pi}\, p_e \exp(-p_e^2) erfc(-ip_e), \tag{1.1d}$$

$$p_e = \sqrt{\frac{1}{2} ikR_2}\,[\beta + \cos(\theta)]. \tag{1.1e}$$

Here ϕ is the acoustic potential, $k = \omega/c$ is the wave number, ω is the circular frequency, c is the characteristic sound speed in air, R_1 is the path length between the source and the receiver, R_2 is the path length between the image source and the receiver, Q is the spherical wave reflection coefficient, $R(\theta)$ is the plane wave reflection coefficient, θ is the angle of incidence measured from the normal axis of the impedance surface, β is the acoustic admittance, $F(p_e)$ is the boundary loss factor, p_e is the numerical distance, and $erfc(-ip_e)$ is the complementary error function with complex argument. Daigle and Stinson proposed the procedure of the phase difference technique to acquire the impedance,[6] but the results showed a wide range of uncertainties at frequencies below $200Hz$. Davies and Mulholland utilized the pulse method to determine the normal impedance at oblique incidence.[7] Jones and Stiede compared different methods of measuring the impedance inside an impedance tube.[8]

1.4 Theoretical Literature Review

Theoretical prediction of sound pressure level (SPL) reflected from a homogeneous impedance ground is based on the Weyl Van der Pol formula. Nocke et al.[9] numerically search the acoustic admittance β from the Weyl Van der Pol formula. The admittance β is the inverse of the acoustic impedance Z. An estimated value of β' for β is pre-selected to compute the spherical wave reflection coefficient $Q(\beta')$ from Eq. (1.1b) to Eq. (1.1e). The measured spherical wave reflection coefficient $Q_{measured}$ is deduced from the measured excess attenuation (EA) that has the following expression

$$EA = 20\log_{10}\left|\frac{P_t}{P_d}\right|,$$

$$P_t = P_0\left[\frac{\exp(ikR_1)}{R_1} + Q_{measured}\frac{\exp(ikR_2)}{R_2}\right],$$

$$P_d = P_0\frac{\exp(ikR_1)}{R_1}, \quad P_0 \text{ is a constant.}$$

Here P_d is the direct wave sound pressure level, P_t is the total wave sound pressure level. If $Q(\beta')$ is within certain accuracy when compared with $Q_{measured}$, then the search is terminated. Otherwise, a new search for β is generated by Nelder-Meade method or Downhill Simplex method. The numerical searching process continues until $\left|Q_{measured} - Q_{theoretical}(\beta^*)\right| < tolerance$, where *tolerance* is a small positive real number, or the maximum number of iterations has been reached.

The derivation of the Weyl Van der Pol formula can be found from Brekhovskikh[10] and Chien and Soroka.[11,12] Upon the reflection from the impedance ground, a reliable impedance model is desired. There are many different formulations on acoustic impedance models. Some impedance models are obtained by curve fitting the experimental data. Others depend on material parameters such as porosity, flow

resistivity, turtuosity, etc.[13] By measuring the sound pressure level through experimental procedures, excess attenuation (EA) can be computed with respect to the measured data. Its definition is generally accepted to be $EA = 20\log_{10}\left|\frac{p_t}{p_d}\right|$, p_t and p_d are the total and direct sound pressure field respectively. However, the excess attenuation (EA) at various frequencies depends on source height, receiver height, horizontal separation distance, ground topology and meteorological effects.[14] Once the excess attenuation is known at certain receiver points, we can formulate the acoustic impedance model of the reflecting surface. With a known impedance model, we can then calculate the sound pressure level over the whole domain of interest either numerically or theoretically. Prediction of sound pressure field by Weyl Van der Pol formula and impedance model assumes a locally reacting surface. Experimental comparisons on monopole and dipole making use of Weyl Van der Pol formula and two-parameter impedance model can be found from Li et al.[15] If the acoustic surface is of extended reaction, the reflection coefficient becomes dependent on the angle of incidence θ. Unfortunately, analytical method of solving acoustic problem with extended reaction ground has not been known yet. Nonetheless, the time-domain numerical approach could provide a mean of unraveling the mystery.

1.5 Numerical Literature Review

Time-domain construction of specific acoustic impedance has drawn much attention recently. The validity of the time-domain impedance boundary condition can be established from the comparison between numerical solutions and frequency-domain solutions. Until recently, numerical implementation of the acoustic impedance in time-domain has yet been performed. However, if the time-domain impedance

boundary condition is verified to be equivalent to the frequency-domain impedance boundary condition, specific acoustic impedance can then be accessed numerically. Fung and Tallapragada[16] formulated the frequency-domain reflection coefficient $\hat{W}(\omega)$ as a ratio of the reflected wave to the incident wave. The formulation is $\hat{u}^- = \hat{W}(\omega)\hat{u}^+$ at the impedance boundary, where $\hat{u}^+ = \hat{u} + \hat{p}$ and $\hat{u}^- = \hat{u} - \hat{p}$, $\hat{u}$ and $\hat{p}$ are the Fourier components of the acoustic normal velocity u and the acoustic pressure p respectively. The frequency-domain reflection coefficient $\hat{W}(\omega)$ is defined as

$$\hat{W}(\omega) = \frac{1 - Z(\omega)}{1 + Z(\omega)}, \tag{1.2}$$

where $Z(\omega) = R_0(\omega) + iX_0(\omega)$ is the impedance of the reflecting surface and ω is the circular frequency of the incident wave, $R_0(\omega)$ is the resistance of the impedance, $X_0(\omega)$ is the reactance of the impedance. The corresponding time-domain formulation of $\hat{W}(\omega)$ for single frequency Ω is

$$W\left(\frac{d}{idt}\right) = U(\Omega) + V(\Omega)\frac{d}{\Omega dt}, \tag{1.3a}$$

$$U = \frac{1 - R_0^2 - X_0^2}{(1 + R_0)^2 + X_0^2}, \tag{1.3b}$$

$$V = -\frac{2X_0}{(1 + R_0)^2 + X_0^2}. \tag{1.3c}$$

The value of the impedance $Z(\omega)$ is obtained experimentally. For the 6.7%-perforated treatment panel,[17] its $U(\omega)$ and $V(\omega)$ representations in $\hat{W}(\omega) = U(\omega) + iV(\omega)$ by least square fitting may be expressed as

$$U(\omega) = -1.1877 + 0.8918\omega^2 - 0.1349\omega^4 + 0.005916\omega^6,$$

$$V(\omega) = 1.074\omega + 0.2921\omega^3 - 0.01586\omega^5.$$

Tam and Auriault used the usual definition for impedance,[17] which is the ratio of the acoustic pressure to the acoustic normal velocity. They proposed the time-domain formulation of the surface impedance for acoustic wave with single frequency Ω as

$$\frac{\partial p}{\partial t} = R_0 \frac{\partial u}{\partial t} - X_0 \Omega u, \qquad X_0 < 0, \tag{1.4a}$$

$$p = R_0 u + \frac{X_0}{\Omega} \frac{\partial u}{\partial t}, \qquad X_0 \geq 0, \tag{1.4b}$$

where p is the acoustic pressure and u is the acoustic velocity normal to the impedance surface, Ω is the frequency of the incidence wave. The separated consideration of the negative and non-negative reactance X_0 is because of numerical stability. The Fourier transform of Eq. (1.4) will give the frequency-domain impedance boundary condition. The acoustic resistance R_0 and the acoustic reactance X_0 are generally frequency dependent. They also vary with the intensity of the incident sound wave and the adjacent mean flow velocity.[17]

Glandier et al.[18] employed the BEM for the sound fields inside a rectangular cavity with impedance treatment on one of its interior surfaces. Numerous high-order accurate finite difference schemes representing the governing equation in the domain of interest, the initial conditions and the boundary conditions have been used to attaining solutions for the wave problem. Sparrow used the Lattice gas method in the aeroacoustics computation.[19] Kim and Roe recommended the second and fourth-order upwind leapfrog schemes to tackle the acoustic equations in polar coordinates.[20] Goodrich applied a new finite difference method to the linearized two-dimensional Euler equation.[21] Tang and Baeder suggested the Cubic-Interpolated Psuedo-particle (CIP) scheme for the linear convection equation.[22] This method is a polynomial interpolant representation of the grid cell. Tam and Webb constructed a dispersion relation preserving (DPR) scheme.[23] The scheme is a finite difference scheme with

the same dispersion relation as the PDE that is being studied. Carpenter et al. proposed a compact scheme that is both GKS and asymptotically stable.[24] In addition, simultaneous approximation term (SAT) was introduced to better treat the boundary condition.[25] Fung et al. demonstrated the accuracy of the implicit high-order compact scheme to the convection equation and the two-dimensional Euler equation.[26] Boulanger et al. applied the BEM to acoustic problem with mixed impedance ground.[27] The BEM numerical results were compared with mixed impedance models and experimental data. Botteldooren had treated the time-domain acoustic problem by means of the finite volume method.[28,29] But the numerical method was limited only to the particular impedance boundary condition.

1.6 Areas of Investigation

In Chapter 2, acoustic wave equation in two dimensions with time-domain impedance boundary condition will be formulated. Analytical methods of deriving the time-domain impedance boundary condition from the frequency-domain impedance boundary condition for the multi-dimensional problems will be covered. In Chapter 3, the one-dimensional piston problem bounded at two ends is presented. One-dimensional wave equation with impedance boundary condition is dealt with by both frequency-domain and time-domain approaches. The time-domain impedance boundary condition is coded into the Compact 3rd order Non-uniform grid[26] (C3N) numerical scheme. Impedance values at different frequencies will be extracted from the C3N numerical results and compared with the theoretical impedance values. In Chapter 4, the reflection of harmonic sound sources from a uniform impedance ground is discussed. The constructed two-dimensional Weyl Van der Pol formula will be compared with the two-dimensional time-domain numerical solution computed

using the C3N finite difference scheme over a homogeneous impedance ground. Comparisons of the time-domain numerical approach on a mixed impedance ground with the existing mixed impedance models will also be shown. Finally, a discussion on the applications and extensions of the time-domain approach to acoustic problems will be given in Chapter 5.

Chapter 2 Time-Domain Formulation

2.1 Governing Equations, Directional Formulation and the C3N Scheme

The linearized isentropic 2-D Euler equations with source terms are written as

$$\frac{\partial U}{\partial t} + A_x \frac{\partial U}{\partial x} + A_y \frac{\partial U}{\partial y} = S, \tag{2.1}$$

where

$$U = \begin{bmatrix} u \\ v \\ p \end{bmatrix}, \quad A_x = \begin{bmatrix} M_x & 0 & 1 \\ 0 & M_x & 0 \\ 1 & 0 & M_x \end{bmatrix}, \quad A_y = \begin{bmatrix} M_y & 0 & 0 \\ 0 & M_y & 1 \\ 0 & 1 & M_y \end{bmatrix}, \quad S = \begin{bmatrix} f_x \\ f_y \\ f_\rho \end{bmatrix},$$

where p is the perturbed pressure from the ambient pressure p_0, u and v are the perturbed velocities from the ambient velocities U and V in x and y directions respectively, $M_x = U/c$ and $M_y = V/c$ are Mach number components in the x and y directions respectively, c is the sound speed of air. Sound sources involved are the oscillating forces $\bar{f} = (f_x, f_y)^T$ and the injection or expansion of fluid force f_ρ in the forms of dipoles and monopoles. Density, length, velocity components, time and sound pressure level have been non-dimensionalized by the ambient density ρ_0, the characteristic length L, the sound speed c, the characteristic time L/c, and the dynamic pressure $\rho_0 c^2$ respectively. Since no heat is added or removed from the system, the flow is adiabatic. Further, with no viscous dissipation, entropy change is non-existent. That means the flow system is a reversible process. An isentropic process is both adiabatic and reversible. Following Fung et al.,[26] Eq. (2.1) is split into two sets of equations

$$\frac{\partial U}{\partial t} + A_x \frac{\partial U}{\partial x} = \frac{S}{2}, \qquad \frac{\partial U}{\partial t} + A_y \frac{\partial U}{\partial y} = \frac{S}{2}.$$

The source S assumes the average strength in each direction for algorithmic symmetry. Each of the above equation sets can further be diagonalized and decoupled.

In the x-direction,

$$\frac{\partial}{\partial t}\begin{bmatrix} v \\ u-p \\ u+p \end{bmatrix}+\begin{bmatrix} M_x & 0 & 0 \\ 0 & M_x-1 & 0 \\ 0 & 0 & M_x+1 \end{bmatrix}\frac{\partial}{\partial x}\begin{bmatrix} v \\ u-p \\ u+p \end{bmatrix}=\frac{1}{2}\begin{bmatrix} f_y \\ f_x-f_\rho \\ f_x+f_\rho \end{bmatrix}. \tag{2.2a}$$

In the y-direction,

$$\frac{\partial}{\partial t}\begin{bmatrix} u \\ v-p \\ v+p \end{bmatrix}+\begin{bmatrix} M_y & 0 & 0 \\ 0 & M_y-1 & 0 \\ 0 & 0 & M_y+1 \end{bmatrix}\frac{\partial}{\partial y}\begin{bmatrix} u \\ v-p \\ v+p \end{bmatrix}=\frac{1}{2}\begin{bmatrix} f_x \\ f_y-f_\rho \\ f_y+f_\rho \end{bmatrix}. \tag{2.2b}$$

Thus waves in 2-D are split into 6 simple waves (or 4 simple waves, $M_x = M_y = f_x = f_y = 0$), each of which has the form

$$\frac{\partial \Theta}{\partial t}+M\frac{\partial \Theta}{\partial \sigma}=s. \tag{2.3}$$

Eq. (2.3) is discretized using the C3N scheme,[26]

$$a_0\Theta_j^{n+1}+a_1\Theta_{j-1}^{n+1}+a_2\Theta_{j+1}^{n+1}=b_0\Theta_j^n+b_1\Theta_{j-1}^n+b_2\Theta_{j+1}^n+\Delta t(a_m s_{j-1}^{n+\frac{1}{2}}+as_j^{n+\frac{1}{2}}+a_p s_{j+1}^{n+\frac{1}{2}}), \tag{2.4}$$

where

$$a_0=a+\frac{\upsilon b}{2}, \qquad a_1=a_m+\frac{\upsilon b_m}{2}, \qquad a_2=a_p+\frac{\upsilon b_p}{2},$$

$$b_0=a-\frac{\upsilon b}{2}, \qquad b_1=a_m-\frac{\upsilon b_m}{2}, \qquad b_2=a_p-\frac{\upsilon b_p}{2},$$

$$a_m=\frac{r^2}{(r+1)^2}, \qquad a=1, \qquad a_p=\frac{1}{(r+1)^2},$$

$$b_m=-\frac{2r^2(r+2)}{(r+1)^3}, \qquad b=\frac{2(r-1)}{r}, \qquad b_p=\frac{2(2r+1)}{r(r+1)^3},$$

$$\upsilon = M\frac{\Delta t}{\Delta\sigma}, \qquad r = \frac{\Delta\sigma_{j+1}}{\Delta\sigma_j}, \qquad \Delta\sigma_{j+1} = \sigma_{j+1} - \sigma_j .$$

The symbol $\Theta = u$, u-p, u+p, v, v-p or v+p, with corresponding $M = M_x$, M_x-1, M_x+1, M_y, M_y-1, or M_y+1. The corresponding $s = f_x/2$, $(f_x-f_\rho)/2$, $(f_x+f_\rho)/2$, $f_y/2$, $(f_y-f_\rho)/2$ or $(f_y+f_\rho)/2$, $\sigma = x$ when Eq. (2a) is used, $\sigma = y$ when Eq. (2b) is used. Though the current form pertains to two-dimensional problems, the directional splitting of the three-dimensional problem is straightforward and shown below.

The linearized isentropic 3-D Euler equations with source terms are written as

$$\frac{\partial U}{\partial t} + A_x\frac{\partial U}{\partial x} + A_y\frac{\partial U}{\partial y} + A_z\frac{\partial U}{\partial z} = S ,$$

where

$$U = \begin{bmatrix} u \\ v \\ w \\ p \end{bmatrix}, \qquad A_x = \begin{bmatrix} M_x & 0 & 0 & 1 \\ 0 & M_x & 0 & 0 \\ 0 & 0 & M_x & 0 \\ 1 & 0 & 0 & M_x \end{bmatrix}, \qquad A_y = \begin{bmatrix} M_y & 0 & 0 & 0 \\ 0 & M_y & 0 & 1 \\ 0 & 0 & M_y & 0 \\ 0 & 1 & 0 & M_y \end{bmatrix},$$

$$A_z = \begin{bmatrix} M_z & 0 & 0 & 0 \\ 0 & M_z & 0 & 0 \\ 0 & 0 & M_z & 1 \\ 0 & 0 & 1 & M_z \end{bmatrix}, \qquad S = \begin{bmatrix} f_x \\ f_y \\ f_z \\ f_\rho \end{bmatrix}.$$

The perturbed velocity vector $\bar{u} = (u, v, w)$ and the perturbed sound pressure p have been non-dimensionalized by the sound speed c and the dynamic pressure $\rho_0 c^2$ respectively, ρ_0 is the ambient density of air, $M_x = U/c$, $M_y = V/c$ and $M_z = W/c$ are Mach number components in the x, y and z directions respectively, $\bar{U} = (U, V, W)$ is the ambient mean velocity vector. Sound sources involved are the oscillating forces $\bar{f} = (f_x, f_y, f_z)$ and

injection or expansion of fluid force f_ρ in the forms of dipoles and monopoles. Following Fung et al.,[26] the 3-D Euler equation is split into three sets of equation

$$\frac{\partial U}{\partial t} + A_x \frac{\partial U}{\partial x} = \frac{S}{3}, \qquad \frac{\partial U}{\partial t} + A_y \frac{\partial U}{\partial y} = \frac{S}{3}, \qquad \frac{\partial U}{\partial t} + A_z \frac{\partial U}{\partial z} = \frac{S}{3}.$$

The source S assumes the average strength in each direction for algorithmic symmetry. Each of the above equation sets can further be diagonalized and decoupled.

In the x direction,

$$\frac{\partial}{\partial t}\begin{bmatrix} v \\ w \\ u-p \\ u+p \end{bmatrix} + \begin{bmatrix} M_x & 0 & 0 & 0 \\ 0 & M_x & 0 & 0 \\ 0 & 0 & M_x - 1 & 0 \\ 0 & 0 & 0 & M_x + 1 \end{bmatrix} \frac{\partial}{\partial x}\begin{bmatrix} v \\ w \\ u-p \\ u+p \end{bmatrix} = \frac{1}{3}\begin{bmatrix} f_y \\ f_z \\ f_x - f_\rho \\ f_x + f_\rho \end{bmatrix}.$$

In the y direction,

$$\frac{\partial}{\partial t}\begin{bmatrix} w \\ u \\ v-p \\ v+p \end{bmatrix} + \begin{bmatrix} M_y & 0 & 0 & 0 \\ 0 & M_y & 0 & 0 \\ 0 & 0 & M_y - 1 & 0 \\ 0 & 0 & 0 & M_y + 1 \end{bmatrix} \frac{\partial}{\partial y}\begin{bmatrix} w \\ u \\ v-p \\ v+p \end{bmatrix} = \frac{1}{3}\begin{bmatrix} f_z \\ f_x \\ f_y - f_\rho \\ f_y + f_\rho \end{bmatrix}.$$

In the z direction,

$$\frac{\partial}{\partial t}\begin{bmatrix} u \\ v \\ w-p \\ w+p \end{bmatrix} + \begin{bmatrix} M_z & 0 & 0 & 0 \\ 0 & M_z & 0 & 0 \\ 0 & 0 & M_z - 1 & 0 \\ 0 & 0 & 0 & M_z + 1 \end{bmatrix} \frac{\partial}{\partial z}\begin{bmatrix} u \\ v \\ w-p \\ w+p \end{bmatrix} = \frac{1}{3}\begin{bmatrix} f_x \\ f_y \\ f_z - f_\rho \\ f_z + f_\rho \end{bmatrix}.$$

Thus waves in 3-D are split into 12 simple waves (or 6 simple waves, $M_x = M_y = M_z = f_x = f_y = f_z = 0$), each of which has the form of Eq. (2.3) and is handled numerically by Eq. (2.4).

2.2 *Boundary Conditions for the C3N Scheme*

Each simple wave of Eq. (2.3) assumes an updated value at wave entry and is allowed to exit freely through a closure scheme.[26] There are right propagating waves if $M > 0$ and left propagating waves if $M < 0$ in both of the x and y directions of Eq. (2.3). For each simple wave, the C3N scheme requires the information of the values at all grid points at time level n, the boundary value of the entering wave at time level n+1 and the boundary value of the exiting wave at time level n+1 to compute the values of the interior grid points at time level n+1. Whereas the initial ($n = 0$) values at all grid points are known. The entering waves boundary values at time level n+1 are determined according to the boundary conditions. While the exiting waves boundary values are determined according to the characteristic lines of propagation.

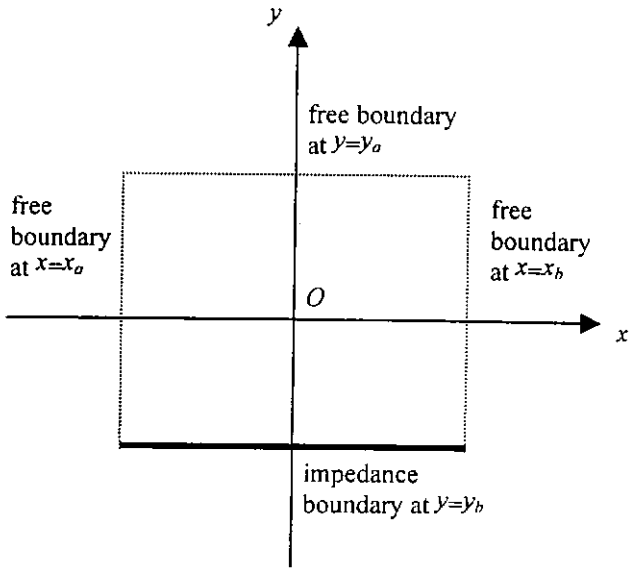

Fig. 2.1. The figure shows the computational domain employed by the C3N numerical scheme with free and impedance boundaries.

Fig. 2.1 shows the computational domain of the two-dimensional reflection problem employed by the C3N scheme. The sound source is placed at the origin O. For the two-dimensional reflection problem, the impedance boundary is at $y=y_b$ and the free

boundaries are at $y=y_a$, $x=x_a$, and $x=x_b$ of the computational domain. Let the domain-exiting wave and the domain-entering wave be v^+ and v^- respectively, v^- is updated at time level $n+1$ by the time-domain equivalent of $\hat{v}^- = \hat{W}(\omega)\hat{v}^+$. Here $\hat{W}(\omega)$ is the frequency-domain reflection coefficient of the acoustic material at the impedance boundary and $\hat{W}(\omega) = 0$ for the free boundaries. The determination of the entering wave v^- at the impedance boundary using the time-domain equivalent of the frequency-domain reflection coefficient $\hat{W}(\omega)$ will be discussed in Section 2.4. For a full description on the evaluation of the exiting wave v^+ at the free boundary in time-domain, please refer to Fung et al.[26]

2.3 Boundary Schemes and Numerical Stability

When free boundary or rigid boundary condition is imposed, there is no numerical stability concerns in the numerical computations. However, if the boundary is of impedance nature, then the impedance boundary condition might give rise to a stability concern. The implementation of the time-domain impedance boundary condition in the C3N scheme is based on the frequency-domain impedance boundary condition. The frequency-domain impedance boundary condition is known to be $\hat{p} = Z(\omega,\theta)\hat{v}$, $\hat{p}$ is the Fourier component of the pressure p, $\hat{v}$ is the Fourier component of the normal velocity v in the y-direction, $Z(\omega,\theta)$ is the frequency-domain acoustic impedance. For simplicity, locally reacting surface is assumed. Hence $Z = Z(\omega)$, which is independent of the angle of incidence θ. Since the wave is reflected at $y=y_b$, the incident wave v^+ and the reflected wave v at the impedance boundary are related by

$$\hat{v}^-(y = y_b) = \hat{W}(\omega)\hat{v}^+(y = y_b), \tag{2.5}$$

where y_b is the right end coordinate value in the y-direction, $\hat{v}^+ = \hat{v} + \hat{p}$ and $\hat{v}^- = \hat{v} - \hat{p}$.

The frequency-domain reflection coefficient $\hat{W}(\omega)$ is related to the impedance $Z(\omega)$ by

$$\hat{W}(\omega) = \frac{1 - Z(\omega)}{1 + Z(\omega)}. \tag{2.6}$$

Taking the modulus on both sides of Eq. (2.6), we have

$$\left|\hat{W}(\omega)\right| = \left|\frac{1 - Z(\omega)}{1 + Z(\omega)}\right|$$

$$= \frac{\left|1 - R_0 - iX_0\right|}{\left|1 + R_0 + iX_0\right|}, \qquad Z(\omega) = R_0 + iX_0,$$

$$= \frac{\sqrt{1 - 2R_0 + R_0^2 + X_0^2}}{\sqrt{1 + 2R_0 + R_0^2 + X_0^2}}.$$

Therefore, if $Re(Z) = R_0 \geq 0$ then $\left|\hat{W}(\omega)\right| \leq 1$. To scrutinize the stability of the numerical scheme on the interior grid points, we use Fourier (Von Neumann) stability analysis. Eq. (2.4) without the source term is

$$a_0\Theta_j^{n+1} + a_1\Theta_{j-1}^{n+1} + a_2\Theta_{j+1}^{n+1} = b_0\Theta_j^n + b_1\Theta_{j-1}^n + b_2\Theta_{j+1}^n. \tag{2.8}$$

By substituting $\Theta_j^n = e^{i\omega n\Delta t + ikj\Delta\sigma}$ into Eq. (2.8) and assuming uniform grid, i.e. $r = \frac{\Delta\sigma_{j+1}}{\Delta\sigma_j} = 1$ in Eq. (2.4), the amplification factor G of Eq. (2.8) becomes

$$G = e^{i\omega\Delta t} = \frac{b_0 + b_1e^{-ik\Delta\sigma} + b_2e^{ik\Delta\sigma}}{a_0 + a_1e^{-ik\Delta\sigma} + a_2e^{ik\Delta\sigma}}.$$

To show the numerical stability on the interior grid points, we need $|G| \leq 1$. From Eq. (2.4) when $r = 1$,

$$a_0 = 1, \qquad a_1 = \frac{1}{4} - \frac{3\upsilon}{8}, \qquad a_2 = \frac{1}{4} + \frac{3\upsilon}{8},$$

$$b_0 = 1, \qquad b_1 = \frac{1}{4} + \frac{3\upsilon}{8}, \qquad b_2 = \frac{1}{4} - \frac{3\upsilon}{8}.$$

As a result,

$$G = \frac{1 + \alpha\cos(k\Delta\sigma) + \beta\cos(k\Delta\sigma) + i[-\alpha\sin(k\Delta\sigma) + \beta\sin(k\Delta\sigma)]}{1 + \alpha\cos(k\Delta\sigma) + \beta\cos(k\Delta\sigma) + i[\alpha\sin(k\Delta\sigma) - \beta\sin(k\Delta\sigma)]},$$

where

$$\alpha = a_2 = b_1 = \frac{1}{4} + \frac{3\upsilon}{8}, \qquad \beta = a_1 = b_2 = \frac{1}{4} - \frac{3\upsilon}{8}.$$

Taking the modulus of G, we obtain

$$|G| = \frac{\sqrt{[1 + \alpha\cos(k\Delta\sigma) + \beta\cos(k\Delta\sigma)]^2 + [-\alpha\sin(k\Delta\sigma) + \beta\sin(k\Delta\sigma)]^2}}{\sqrt{[1 + \alpha\cos(k\Delta\sigma) + \beta\cos(k\Delta\sigma)]^2 + [\alpha\sin(k\Delta\sigma) - \beta\sin(k\Delta\sigma)]^2}} = 1.$$

Thus, the scheme is stable on both the interior and impedance boundary grid points.

2.4 Time-Domain Impedance Boundary Condition

To obtain the time-domain reflected wave v^- from the time-domain incident wave v^+ at the impedance boundary, inverse Fourier transform and convolution theorem are applied toward Eq. (2.5). The result gives

$$v^-(t) = \int_{-\infty}^{\infty} W(t-\tau)v^+(\tau)\mathrm{d}\tau. \tag{2.9}$$

$W(t)$ is the inverse Fourier transform component of $\hat{W}(\omega)$ defined in Eq. (2.6). The expression in Eq. (2.9) involves an infinitely time integration as a result of the inverse Fourier transform. This integration is not immediately applicable to time-domain methods unless the integration period can be localized. The behaviors of $W(t)$ depend on

$Z(\omega)$, which is primarily an experimental quantity and may not be an analytic function of ω. Consider a simple Fourier transformed three-parameter frequency-domain impedance model,

$$Z(\omega)=R_0+iX_0 =R_0+i(X_{-1}/\omega+X_1\omega). \tag{2.10}$$

This impedance $Z(\omega)$ contains the real part of resistance R_0 and the imaginary part of reactance X_0. The parameters R_0, X_{-1}, X_1 are predefined real coefficients that give the best fit of the ground impedance over a range of frequencies. This algebraic model describes a class of sound absorptive materials with constant resistance that has linearly varying reactance at high frequency and inversely linearly varying reactance at low frequency. For a 6.7%-perforate treatment panel,[17] the best fit parameters are experimentally found to be $R_0 = 0.2$, $X_{-1} = -13.48$, $X_1 = 0.739$ in Eq. (2.10). The unit of the dimensional ω is measured in kilo-radian per second. R_0 and X_0 are non-dimensional but X_{-1} is dimensional with the same unit of ω and X_1 is dimensional with the inverse unit of ω. If ω is non-dimensionalized by the characteristic time L/c, where $L = 0.01m$ is the characteristic length and $c = 340m/s$ is the characteristic velocity, then $R_0 = 0.2$, $X_{-1} = -0.396471$, $X_1 = 2.5126$ are all non-dimensional quantities. From Eq. (2.6), the time-domain reflection coefficient becomes,

$$W(t) = \frac{1}{2\pi}\int_{-\infty}^{\infty}\frac{1-Z(\omega)}{1+Z(\omega)}\exp(i\omega t)d\omega$$

$$= \frac{1}{2\pi}\int_{-\infty}^{\infty}\frac{1-R_0-i\left(\frac{X_{-1}}{\omega}+X_1\omega\right)}{1+R_0+i\left(\frac{X_{-1}}{\omega}+X_1\omega\right)}\exp(i\omega t)d\omega$$

$$= \frac{1}{2\pi}\int_{-\infty}^{\infty}\left[\frac{2\frac{\omega}{X_1}}{i\left(\omega^2 - i2\frac{1+R_0}{2X_1}\omega + \frac{X_{-1}}{X_1}\right)} - 1\right]\exp(i\omega t)d\omega$$

$$= \frac{1}{2\pi}\int_{-\infty}^{\infty}\frac{2\frac{\omega}{X_1}}{i(\omega-\omega_1)(\omega-\omega_2)}\exp(i\omega t)d\omega - \delta(t),$$

with

$$\omega_{1,2} = \pm\omega_R + i\omega_I,$$

$$\omega_R = \sqrt{\frac{-X_{-1}}{X_1} - \left(\frac{1+R_0}{2X_1}\right)^2},$$

$$\omega_I = \frac{1+R_0}{2X_1}.$$

By residual theorem,

$$W(t) = \frac{2}{X_1}\left[\frac{\omega_1\exp(i\omega_1 t)}{(\omega_1-\omega_2)} + \frac{\omega_2\exp(i\omega_2 t)}{(\omega_2-\omega_1)}\right] - \delta(t),\ \omega_I > 0,\ t > 0,$$

$$= \frac{2}{X_1}\left[\cos(\omega_R t) - \frac{\omega_I}{\omega_R}\sin(\omega_R t)\right]\exp(-\omega_I t) - \delta(t),\ \omega_I > 0,\ t > 0,$$

and

$$W(t) = -\delta(t),\ \omega_I > 0,\ t < 0.$$

Hence,

$$W(t) = \frac{2H(t)}{X_1}\left[\cos(\omega_R t) - \frac{\omega_I}{\omega_R}\sin(\omega_R t)\right]\exp(-\omega_I t) - \delta(t),\ \omega_I > 0,$$

or equivalently,

$$W(t) = \frac{2H(t)}{X_1}\sqrt{1+\left(\frac{\omega_I}{\omega_R}\right)^2}\cos(\omega_R t + \chi)\exp(-\omega_I t) - \delta(t),\ \omega_I > 0. \qquad (2.11a)$$

$H(t)$ is the Heaviside function which is defined as 1 when $t > 0$ and is defined as 0 when $t < 0$, $\delta(t)$ is the Dirac delta function with $\int_{-\infty}^{\infty} f(t)\delta(t-t_0)dt = f(t_0)$ and $\chi = \tan^{-1}\frac{\omega_I}{\omega_R}$.

Similarly for $\omega_I < 0$,

$$W(t) = \frac{2[1-H(t)]}{X_1}\sqrt{1+\left(\frac{\omega_I}{\omega_R}\right)^2}\cos(\omega_R t + \chi)\exp(-\omega_I t) - \delta(t)\ ,\ \omega_I < 0. \qquad (2.11b)$$

The first term of $W(t)$ in Eq. (2.11) oscillates at frequency $\frac{\omega_R}{2\pi}$ with amplitude

$$\frac{2}{X_1}\sqrt{1+\left(\frac{\omega_I}{\omega_R}\right)^2}\exp(-\omega_I t), \qquad (2.12)$$

which has a decay rate of ω_I. This amplitude is a monotonic function of t. By defining $W_\delta(t) = W(t) + \delta(t)$, we can construct a sequence $\{W_\delta(t_n)\}_{n=0}^{\infty}$. Hence given $\varepsilon > 0$, $\exists N \in [0,\infty)$ s.t. $\forall n > N$, we have $|W_\delta(t_n) - W_\delta(t_\infty)| < \varepsilon$. In other words, $\lim_{n\to\infty} W_\delta(t_n) = W_\delta(t_\infty)$.

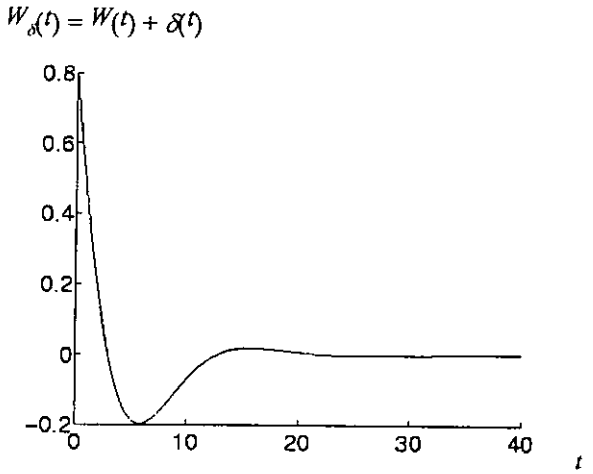

Fig. 2.2. The figure shows the asymptotically decaying property of the function $W_\delta(t)$.

A typical plot of $W_\delta(t) = W(t) + \delta(t)$ is shown in Fig. 2.2. If the asymptotic values of the reflection coefficient $W_\delta(t)$ is negligible beyond certain time T when $|W_\delta(t)|$ dips below a small positive value ε, then there exists compact supports Γ^+ and Γ^-, such that

$$\Gamma^+(t) = \begin{cases} 1, & 0 < t < T, \\ 0, & otherwise, \end{cases}$$

$$\Gamma^-(t) = \begin{cases} 0, & otherwise, \\ 1, & -T < t < 0. \end{cases}$$

Thus Eq. (2.9) may be written as

$$v^-(t) = \int_0^T \Gamma^+(\tau) W_\delta(\tau) v^+(t-\tau)\mathrm{d}\tau - v^+(t), \ \omega_I > 0, \tag{2.13a}$$

$$v^-(t) = \int_{-T}^0 \Gamma^-(\tau) W_\delta(\tau) v^+(t-\tau)\mathrm{d}\tau - v^+(t), \ \omega_I < 0. \tag{2.13b}$$

Eq. (2.13b) corresponds to a non-casual integration which is mathematically plausible but physically unimaginable. By specifying the accuracy required once the amplitude in Eq. (2.12) reaches ε at time T, we obtain

$$\frac{2}{X_1}\sqrt{1+\left(\frac{\omega_I}{\omega_R}\right)^2}\exp(-\omega_I T) = \varepsilon.$$

Hence,

$$T = \frac{1}{\omega_I}\ln\left[\frac{2}{X_1\varepsilon}\sqrt{1+\left(\frac{\omega_I}{\omega_R}\right)^2}\right].$$

The time integration in Eq. (2.13) is a compact implementation of Eq. (2.11). An equivalent discrete form of Eq. (2.13) suitable for the numerical implementation may be written as

$$v^-(t) = \sum_{k=0}^{T/\Delta t} W_\delta(k\Delta t)v^+\left(t-k\Delta t\right) - v^+\left(t\right)\ ,\ \omega_I > 0, \tag{2.14a}$$

$$v^-(t) = \sum_{k=-T/\Delta t}^{0} W_\delta(k\Delta t)v^+\left(t-k\Delta t\right) - v^+\left(t\right)\ ,\ \omega_I < 0. \tag{2.14b}$$

The fact that the wave propagation function $v^+(y,t)$ has the characteristic form $v^+(y-t)$ implies an increase in t by some amount or a decrease in y by the same amount will give the same right traveling phenomenon. Similarly, $v^-(y,t)$ assumes a characteristic form of $v^-(y+t)$ implies an increase in t by some amount or an increase in y by the same amount will give the same left traveling phenomenon. This means the time variation of the flow field at a fixed location is mathematically identical to the spatial variation of a temporally frozen flow. Thus Eq. (2.14) may be formulated alternatively as

$$v^-(y_b,t) = \sum_{k=0}^{T/\Delta y} W_\delta(k\Delta y)v^+\left(y_b+k\Delta y,t\right) - v^+\left(y_b,t\right)\ ,\ \omega_I > 0, \tag{2.15a}$$

$$v^-(y_b,t) = \sum_{k=-T/\Delta y}^{0} W_\delta(k\Delta y)v^+\left(y_b+k\Delta y,t\right) - v^+\left(y_b,t\right)\ ,\ \omega_I < 0, \tag{2.15b}$$

where y_b is the spatial coordinate value of the impedance boundary in the y-direction. Eq. (2.15b) is preferred over Eq. (2.14) because there is no extra spatial storage for $v^-(y,t)$ and $v^+(y,t)$ during the numerical computations.

Notice that the time dependence in the time-domain solution is exp($i\omega t$). This is because exp($i\omega t$) is the convention established in the inverse Fourier transform when determining the time-domain reflection coefficient from the frequency-domain reflection coefficient. However, for outdoor sound propagation, exp(-$i\omega t$) is assumed. As a matter of fact, the

impedance boundary condition for single frequency wave in the Weyl Van der Pol formula when exp(-$i\omega t$) is assumed has long been

$$\hat{p}(r_b,\theta)\exp(-i\omega t) = Z(\omega)\hat{v}(r_b,\theta)\exp(-i\omega t), \tag{2.16}$$

where $\hat{p}(r_b,\theta)$ and $\hat{v}(r_b,\theta)$ are the frequency-domain sound pressure level and the frequency-domain normal velocity at the impedance boundary respectively, r_b is the radial distance from the source to the impedance boundary, θ is the angle of incidence. The complementary counterpart of Eq. (2.16) has exp($i\omega t$) time dependence assumption. This is because the impedance boundary condition complementary to Eq. (2.16) is

$$\overline{\hat{p}(r_b,\theta)}\exp(i\omega t) = \overline{Z(\omega)}\overline{\hat{v}(r_b,\theta)}\exp(i\omega t), \tag{2.17}$$

where $\overline{Z(\omega)}$ is the complex conjugate of the ground impedance $Z(\omega)$, $\overline{\hat{p}(r_b,\theta)}$ and $\overline{\hat{v}(r_b,\theta)}$ are the complex conjugates of their corresponding quantities. By expanding terms, it can be easily shown that Eq. (2.16) and Eq. (2.17) are equivalent to each other. Since exp($i\omega t$) is always assumed in the time-domain numerical solution, the impedance used in the numerical scheme is just the complex conjugate of the impedance being introduced to the Weyl Van der Pol formula where exp(-$i\omega t$) is assumed. If exp($i\omega t$) is assumed in the Weyl Van der Pol formula, both of the impedance inherited to the numerical scheme and the Weyl Van der Pol formula will be the same. Though the solutions of the Weyl Van der Pol formula are complex conjugates to each other with different time dependence assumptions, the prediction on sound pressure level will be the same. After all, only the real part of the Weyl Van der Pol formula is of practicality.

Chapter 3 The One-dimensional Acoustic Problem

3.1 Frequency-Domain Approach

Results of the wave propagation in a piston determined by Laplace transform method is now considered. In this problem, the right end of the piston is being mounted with a sound absorbing material with impedance Z. The impedance Z is in general dependent on the frequencies of the acoustic wave and is assumed to be locally reacting. A physical view on the problem is displayed in Fig. 3.1.

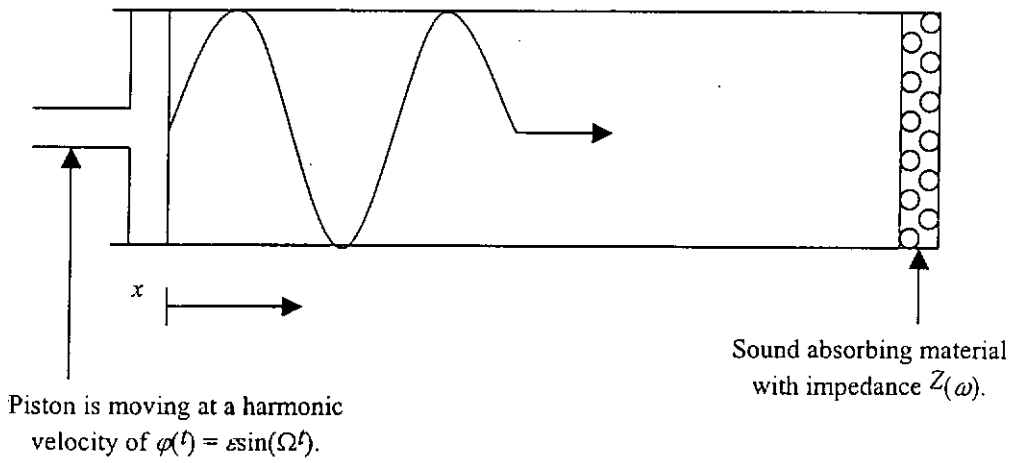

Fig. 3.1. A physical view of the wave propagation inside a piston with impedance material at the right end, ε is the maximum distance of the piston deviates from $x = 0$ with $0 < \varepsilon << 1$.

Non-dimensional spatial variable $x \in [0,1]$ and non-dimensional temporal variable $t \in [0,\infty)$ are assumed. For x in any other interval say $[a,b]$, solution can easily be mapped into the interval $[0,1]$ because (x,t) coordinates can be transformed to (ξ,τ) coordinates by $\xi = (x-a)/(b-a)$ and $\tau = t/(b-a)$ with $\xi \in [0,1]$ and $x \in [a,b]$. Since the piston surface is moving at a velocity $\varphi(t)$, where $\varphi(t) \sim O(\varepsilon)$ and $0 < \varepsilon << 1$, the piston position x_p is related to the piston velocity $\varphi(t)$ by

$$\frac{dx_p}{dt} = \varphi(t).$$

Therefore, $x_p = \int \varphi(t) dt$ is the position of the piston surface as a function of time t.

The left end boundary condition could be regarded as

$$\phi_x(x_p, t) = \varphi(t).$$

By Taylor expanding the left-hand side of the above equation at $x = 0$, we obtain

$$\phi_x(x_p, t) = \phi_x(0, t) + \left(\frac{\partial \phi_x}{\partial x} \right)_{x=0} x_p + \cdots.$$

But

$$\frac{\partial^n \phi_x}{\partial x^n} = \varepsilon \frac{\partial^n}{\partial x^n} [f(x-t) + g(x+t)], \quad n = 1,2,3,\ldots$$

where $f(x-t)$ is the right traveling wave, $g(x+t)$ is the left traveling wave. Both $f(x-t)$ and $g(x+t)$ are functions of $O(1)$. By retaining the $O(\varepsilon)$ terms only, the left end boundary condition becomes

$$\phi_x(0, t) = \varphi(t).$$

The formulation of this 1-D piston problem and the result of the frequency-domain solution are

$$\phi_{tt} - \phi_{xx} = 0, \qquad 0 \le x \le 1, \qquad t > 0, \tag{3.1a}$$

$$\phi(x,0) = 0, \tag{3.1b}$$

$$\phi_t(x,0) = 0, \tag{3.1c}$$

$$\phi_x(0, t) = \varphi(t) H(t), \tag{3.1d}$$

$$-s\hat{\phi}(1, s) = Z(s)\hat{\phi}_x(1, s), \tag{3.1e}$$

where ϕ is the acoustic velocity potential, $\hat{\phi}$ is the Laplace compoent of ϕ, s is the Laplace transform variable in the frequency-domain, $H(t)$ is the Heaviside function, $Z(s)$ is the Laplace transformed three-parameter frequency-domain impedance model which has the form

$$Z(s) = R_0 - \frac{X_{-1}}{s} + X_1 s.$$

R_0, X_{-1}, X_1 are predefined real coefficients that give the best fit of the ground impedance over a range of frequencies. Eq. (3.1e) is the Laplace transformed frequency-domain representation of the impedance boundary condition. By Laplace transform of Eq. (3.1a) to Eq. (3.1d), Eq. (3.1) may be rewritten as

$$\hat{\phi}_{xx} - s^2\hat{\phi} = 0\,, \qquad 0 \le x \le 1,$$

$$\hat{\phi}_x(0,s) = \hat{\varphi}(s),$$

$$-s\hat{\phi}(1,s) = Z(s)\hat{\phi}_x(1,s)\,.$$

The solution of the above ODE is

$$\hat{\phi}(x,s) = A\cosh(sx) + B\sinh(sx),$$

where

$$A = -\hat{\varphi}(s)\frac{\sinh(s) + Z\cosh(s)}{\cosh(s) + Z\sinh(s)}, \qquad B = \hat{\varphi}(s).$$

By inverse Laplace transform,

$$\phi(x,t) = \frac{1}{2\pi i}\int_{\gamma-i\infty}^{\gamma+i\infty}\hat{\phi}(x,s)e^{st}ds$$

$$= \frac{1}{2\pi i}\int_{\gamma-\infty}^{\gamma+\infty}g(x,s)e^{st}ds + \frac{1}{2\pi i}\int_{\gamma-\infty}^{\gamma+\infty}h(x,s)e^{st}ds\,, \qquad (3.2)$$

where

$$g(x,s) = -\hat{\varphi}(s)\frac{\sinh(s) + Z\cosh(s)}{\cosh(s) + Z\sinh(s)}\cosh(sx),$$

$$h(x,s) = \hat{\varphi}(s)\sinh(sx).$$

The value of γ is a chosen real constant such that the contour integration on the complex plane includes all the poles of $g(x,s)$ and $h(x,s)$ that are to the left of the vertical line $x = \gamma$. By choosing $\gamma = 0$, Eq. (3.2) may give a time stable approximation

of Eq. (3.1) after applying the residue theorem in complex analysis. Some of the poles in Eq. (3.2) are determined from

$$\cosh(s) + Z(s)\sinh(s) = 0,$$

or equivalently

$$\frac{e^{2s}+1}{e^{2s}-1} = -Z(s). \tag{3.3}$$

Substituting $s = \alpha_n \pm i\beta_n$ as the poles into Eq. (3.3), the resulting real and imaginary parts are respectively

$$\begin{aligned} &-R_0 e^{2\alpha_n}\cos(2\beta_n) + X_{-1}e^{2\alpha_n}\frac{\alpha_n\cos(2\beta_n)+\beta_n\sin(2\beta_n)}{\alpha_n^2+\beta_n^2} - X_1 e^{2\alpha_n}\left[\alpha_n\cos(2\beta_n)-\beta_n\sin(2\beta_n)\right] \\ &+R_0 - X_{-1}\frac{\alpha_n}{\alpha_n^2+\beta_n^2} + X_1\alpha_n - e^{2\alpha_n}\cos(2\beta_n) - 1 = 0, \end{aligned} \tag{3.4a}$$

and

$$\begin{aligned} &-R_0 e^{2\alpha_n}\sin(2\beta_n) + X_{-1}e^{2\alpha_n}\frac{\alpha_n\sin(2\beta_n)-\beta_n\cos(2\beta_n)}{\alpha_n^2+\beta_n^2} - X_1 e^{2\alpha_n}\left[\alpha_n\sin(2\beta_n)+\beta_n\cos(2\beta_n)\right] \\ &+X_{-1}\frac{\beta_n}{\alpha_n^2+\beta_n^2} + X_1\beta_n - e^{2\alpha_n}\sin(2\beta_n) = 0. \end{aligned} \tag{3.4b}$$

Since $\cos(2\beta_n)$ and $\sin(2\beta_n)$ are periodic functions of β_n with period π, each $\beta_n \in [n\pi, (n+1)\pi]$, where $n = 0,1,2,3,\ldots$, must correspond to a value of α_n so that both satisfy Eq. (3.4). Let ε be a small positive number and $E_n(\alpha_n, \beta_n)$ = L.H.S. of Eq. (3.4a), then for each interval $[n\pi, (n+1)\pi]$, we may use the following algorithm to find α_n and β_n.

1. Set $\beta_n = n\pi$ and $\beta_{n+1} = (n+1)\pi$.
2. With known values of β_n and β_{n+1}, find the corresponding values of α_n and α_{n+1} from Eq. (3.4b) using bisection method.
3. Find $E_n(\alpha_n, \beta_n)$ and $E_{n+1}(\alpha_{n+1}, \beta_{n+1})$.
4. Set $\beta_{n+1/2} = (\beta_n + \beta_{n+1})/2$ and find the corresponding value of $\alpha_{n+1/2}$ from Eq. (3.4b) using bisection method.

5. Find $E_{n+1/2}(\alpha_{n+1/2}, \beta_{n+1/2})$. If $|E_{n+1/2}(\alpha_{n+1/2}, \beta_{n+1/2})| < \varepsilon$ then STOP, take $\alpha_{n+1/2}$ and $\beta_{n+1/2}$ as a root of Eq. (3.4). Otherwise go to Step 6.
6. If $E_n(\alpha_n, \beta_n)$ and $E_{n+1/2}(\alpha_{n+1/2}, \beta_{n+1/2})$ are of opposite signs, set $\beta_{n+1} = \beta_{n+1/2}$, else set $\beta_n = \beta_{n+1/2}$.
7. Go to Step 2.

Once $\varphi(t)$ is known, $\phi(x,t)$ can be evaluated from Eq. (3.2) using convolution theorem.

3.2 Time-Domain Numerical Approach

The acoustic disturbance in a piston is governed by the second order wave equation

$$\frac{\partial^2 \phi}{\partial t^2} - \frac{\partial^2 \phi}{\partial x^2} = f(x,t). \tag{3.5}$$

where $f(x,t)$ is the forcing function, x and t are non-dimensional variables. L must be chosen in a way that the non-dimensional grid size $\Delta x \geq 1$ and there are at least eight grid points per wavelength for each frequency of the wave in the computation. In terms of the potential ϕ, the perturbed velocity u and the perturbed pressure p can be written as $u = \phi_x$ and $p = -\phi_t$ respectively. Similarly, u and p are non-dimensionalized by c and $\rho_0 c^2$ respectively, ρ_0 is the ambient density of air. In terms of u and p, Eq. (3.5) may be written as

$$\frac{\partial U}{\partial t} + A\frac{\partial U}{\partial x} = F, \tag{3.6a}$$

where

$$U = \begin{bmatrix} u \\ p \end{bmatrix}, \qquad A = \begin{bmatrix} 0 & 1 \\ 1 & 0 \end{bmatrix}, \qquad F = \begin{bmatrix} 0 \\ -f \end{bmatrix}. \tag{3.6b}$$

Eq. (3.6) is recognized as the linearized isentropic Euler equations with a source term. It can be transformed into an uncoupled system as

$$\frac{\partial \overline{U}}{\partial t} + \overline{A}\frac{\partial \overline{U}}{\partial x} = \overline{F}, \tag{3.7a}$$

where

$$\overline{U} = \begin{bmatrix} u-p \\ u+p \end{bmatrix}, \qquad \overline{A} = \begin{bmatrix} -1 & 0 \\ 0 & 1 \end{bmatrix}, \qquad \overline{F} = \begin{bmatrix} f \\ -f \end{bmatrix}. \tag{3.7b}$$

The term $u+p$ is known as the advancing wave, $u-p$ is known as the receding wave. The above transformation is based on matrix theory from linear algebra. By assuming matrix A to be diagonalizable, the eigenvectors of matrix A will span the n-dimensional Euclidean space $\Re^n$ with n being the dimension of matrix A. In this case, $n = 2$. Hence there exists a matrix P such that $\overline{A} = P^{-1}AP$. The diagonal elements of matrix $\overline{A}$ are the eigenvalues of matrix A. The off-diagonal elements of matrix $\overline{A}$ are all zeros. Columns of P contains the distinct eigenvectors of matrix A. Thereafter, Eq. (3.6a) can be written as

$$\frac{\partial U}{\partial t} + P\overline{A}P^{-1}\frac{\partial U}{\partial x} = F.$$

Multiplying the above equation throughout by P^{-1}, we then obtain Eq. (3.7). At the left end boundary, say $x=a$, the condition $u(x=a,t) = \varphi(t)H(t)$ is inscribed, $\varphi(t)$ is an arbitrary function, $H(t)$ is the Heaviside function. At the right impedance boundary, say $x=b$, $\hat{p}(x=b,\omega) = Z(\omega)\hat{u}(x=b,\omega)$ is supposed for a locally reacting end. The impedance model employed is the time-domain equivalent of the Fourier transformed three-parameter frequency-domain impedance model. It has the form

$$Z(\omega) = R_0(\omega) + iX_0(\omega) = R_0 + i\left(\frac{X_{-1}}{\omega} + X_1\omega\right).$$

Refering to Fung,[16] the time-domain impedance boundary may be constructed from the frequency-domain relation $\hat{u}^+ = \hat{W}\hat{u}^-$ at the boundary, $\hat{W}$ is the Fourier component of the time-domain reflection coefficient W. The relation between

impedance Z and the frequency-domain reflection coefficient $\hat{W}$ is $Z = \frac{1-\hat{W}}{1+\hat{W}}$. A detailed description of the equivalent formulation of the time-domain impedance boundary condition in terms of the time-domain reflection coefficient W has been elucidated in Chapter 2. Eq. (3.7) contains two equations, each has the form

$$\frac{\partial \Theta}{\partial t} + M \frac{\partial \Theta}{\partial x} = s,$$

and is discretized using the C3N implicit compact scheme

$$a_0\Theta_j^{n+1} + a_1\Theta_{j-1}^{n+1} + a_2\Theta_{j+1}^{n+1} = b_0\Theta_j^n + b_1\Theta_{j-1}^n + b_2\Theta_{j+1}^n + \Delta t(a_m s_{j-1}^{n+\frac{1}{2}} + a s_j^{n+\frac{1}{2}} + a_p s_{j+1}^{n+\frac{1}{2}}). \quad (3.8)$$

The coefficients in Eq. (3.8) are stated completely in Chapter 2, $\Theta = u\text{-}p$ or $u+p$, with corresponding $M = -1$ or 1. The corresponding $s = -f$ or f.

3.3 Comparison of Frequency-Domain and Time-Domain Results

To give a numerical example, we set $\varphi(t) = \sin(\Omega t)H(t)$, the forcing function $f(x,t) = 0$, parameters for the impedance model Z are $R_0 = 0.2$, $X_{-1} = -13.48$ and $X_1 = 0.0739$, non-dimensional length $L = 0.012m$. Fig. 3.2 shows the results predicted by Eq. (3.2) and the C3N scheme at resonance frequency $f = 2.8333kHz$.

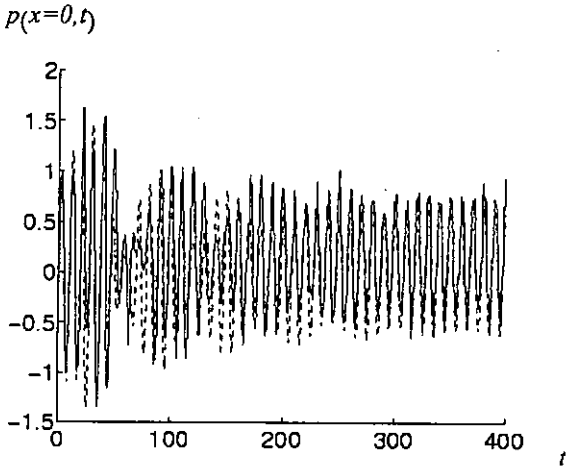

Fig. 3.2. Solid line — is the numerical solution. Dashed line -- is the analytical solution. Frequency is at 2.8333 kHz. Variables x and t are non-dimensional. Length of the piston is 0.12^m. All $\alpha_n < 0$.

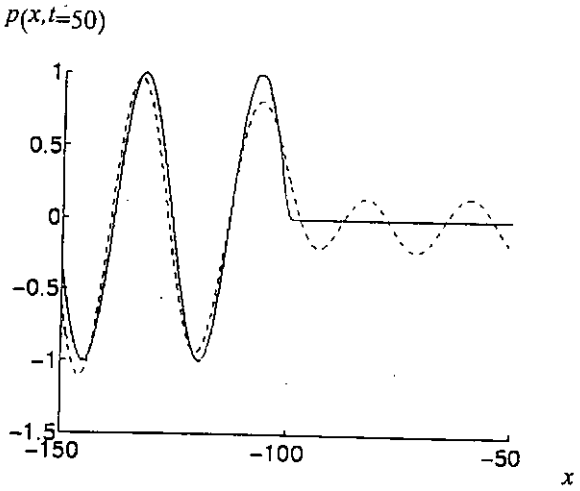

Fig. 3.3 a

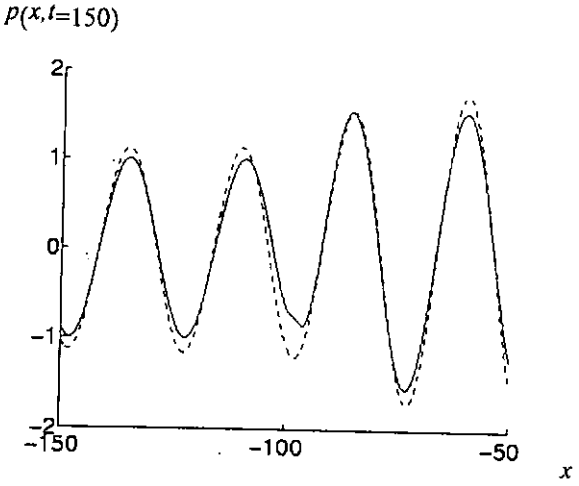

Fig. 3.3 b

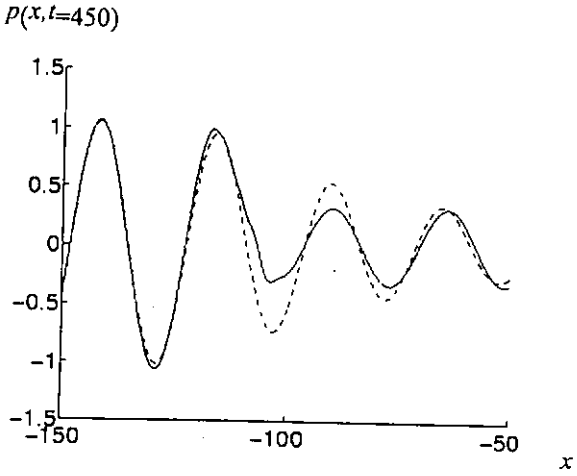

Fig. 3.3 c

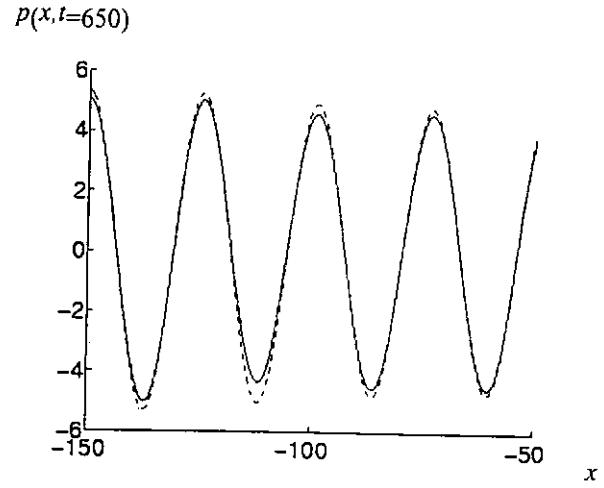

Fig. 3.3 d

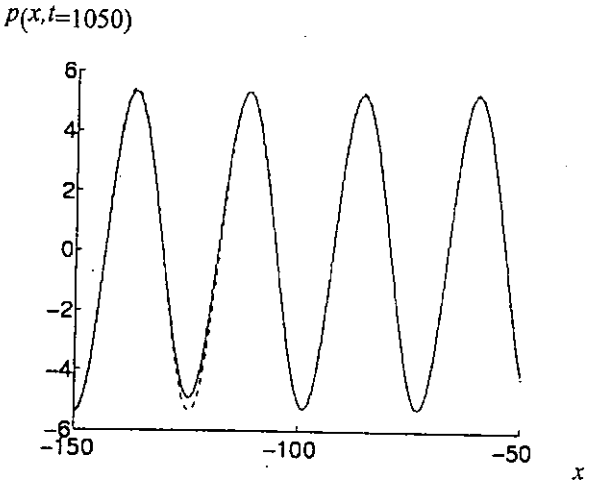

Fig. 3.3 e

Fig. 3.3. The figures have the following configuration. Solid line — is the numerical solution. Dashed line -- is the analytical solution. Frequency is at 1.1 kHz. Variables x and t are non-dimensional. Characteristic length is 0.012^m. All $\alpha_n < 0$.

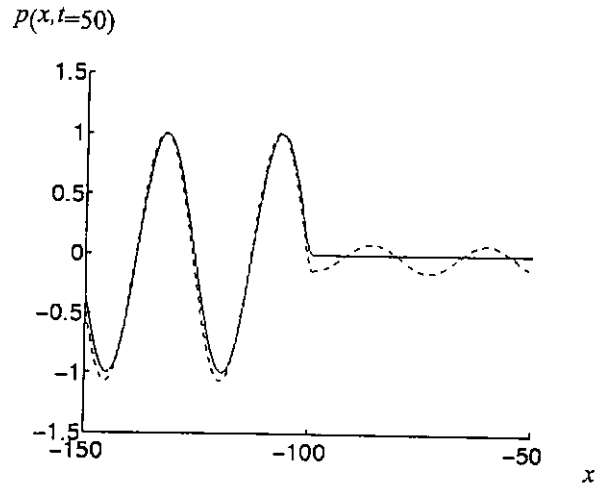

Fig. 3.4 a

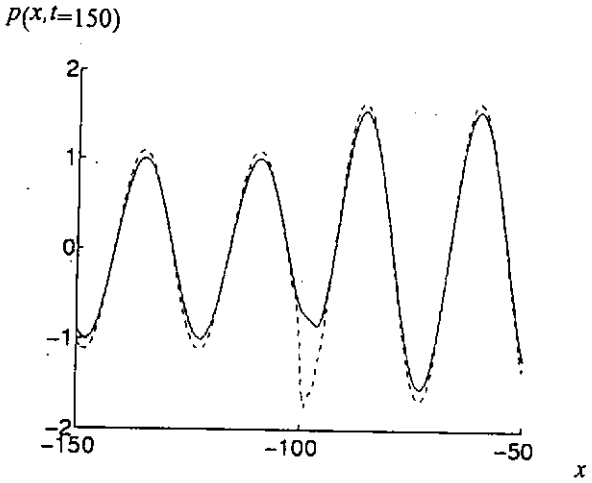

Fig. 3.4 b

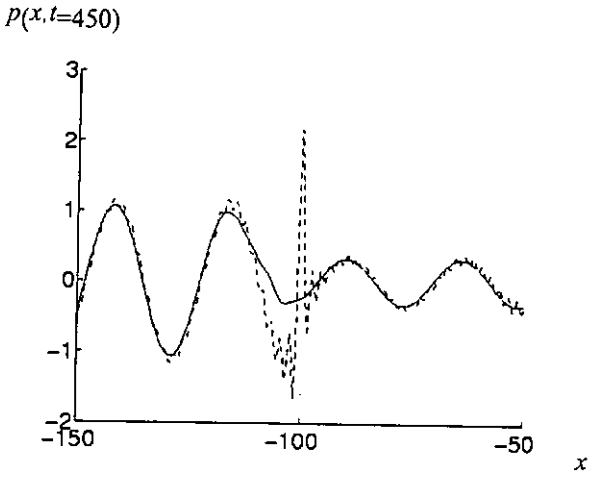

Fig. 3.4 c

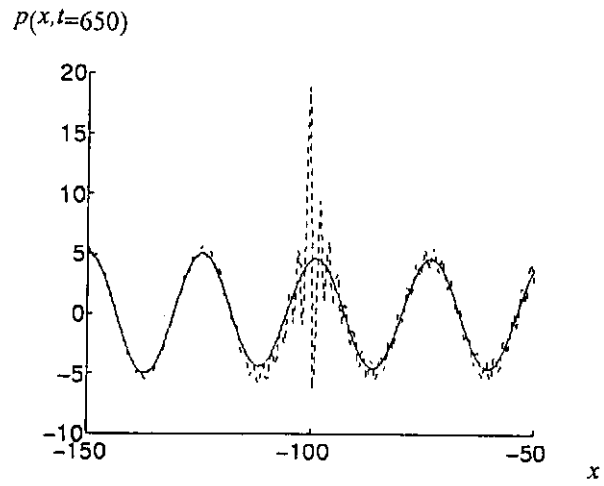

Fig. 3.4 d

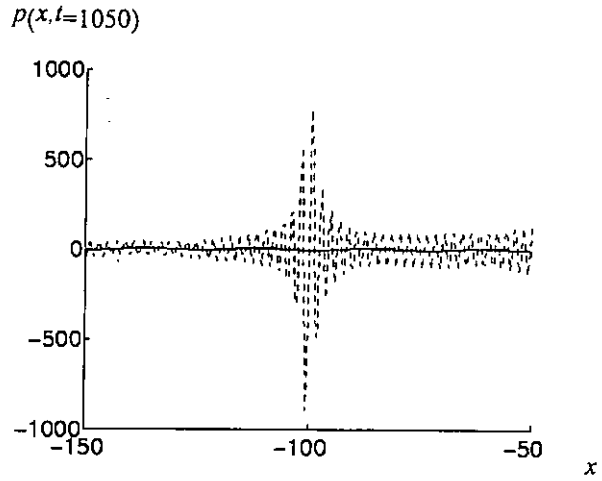

Fig. 3.4 d

Fig. 3.4. The figures have the following configuration. Solid line — is the numerical solution. Dashed line -- is the analytical solution. Frequency is at 1.1 kHz. Variables x and t are non-dimensional. Characteristic length is 0.012^m. Some $\alpha_n > 0$.

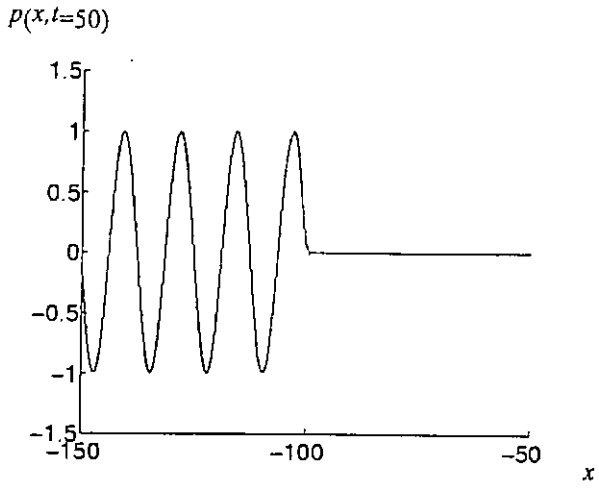

Fig. 3.5 a

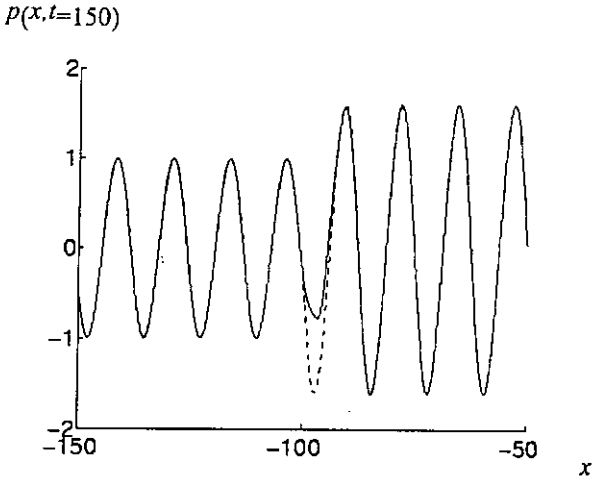

Fig. 3.5 b

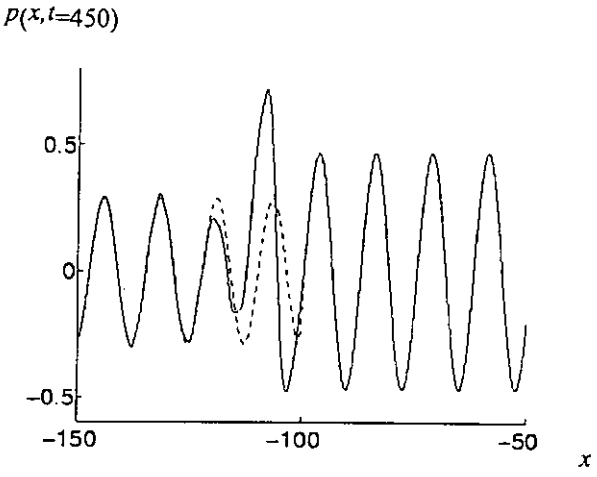

Fig. 3.5 c

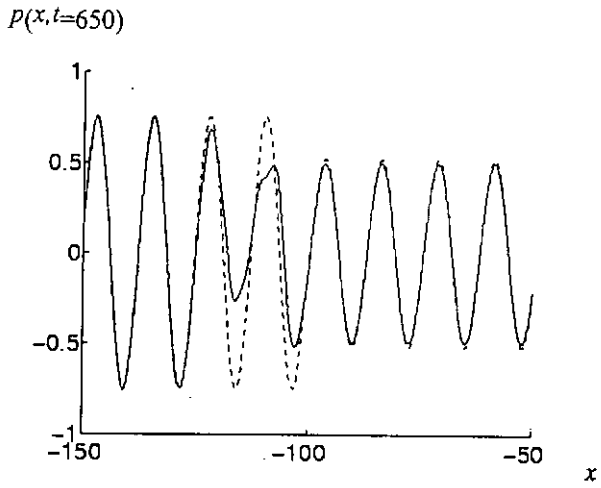

Fig. 3.5 d

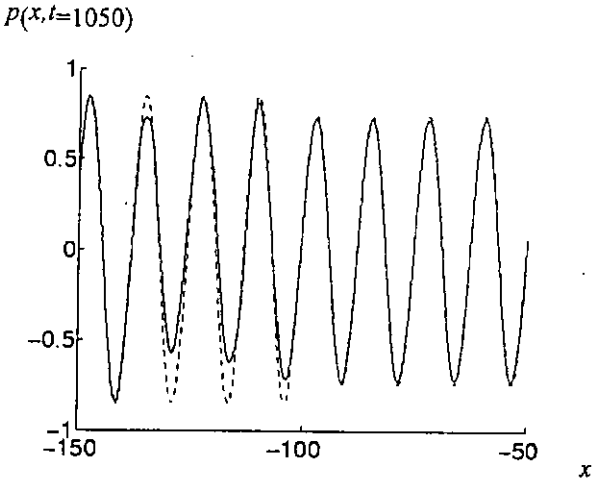

Fig. 3.5 e

Fig. 3.5. The figures have the following configuration. Solid line — is the numerical solution. Dashed line -- is the analytical solution. Frequency is at 2.25 kHz. Variables x and t are non-dimensional. Characteristic length is 0.012^m. All $\alpha_n < 0$.

The plots in Fig. 3.2, Fig. 3.3 and Fig. 3.5 use the poles of Eq. (3.2) lying to the left of the axis $x = \gamma = 0$. This implies that the real parts of the poles are all negative. While Fig. 3.4 has some of the poles lying to the right of the axis $x = \gamma = 0$. That means some of the real part of the poles are positive, which gives rise to the time unstable approximation.

3.4 Verification of Input and Computed Impedance

In order to demonstrate the effectiveness of the time-domain impedance boundary condition, the impedance values are extracted from the numerical results. Assuming the right running wave $u^+(x,t)$ has the form

$$u^+(x,t) = a\cos[\Omega(x-t)+\alpha], \tag{3.9}$$

the unknowns a and α are the amplitude and phase of the wave respectively, Ω is the non-dimensional circular frequency. Expanding Eq. (3.9), we obtain

$$u^+(x,t) = a\cos[\Omega(x-t)]\cos\alpha - a\sin[\Omega(x-t)]\sin\alpha\,.$$

If two values of the numerically computed $u^+(x,t)$ are known at two different locations x with fixed time t, a and α can be resolved. Similarly, the left running wave $u^-(x,t)$ can be expanded as

$$u^-(x,t) = b\cos[\Omega(x+t)]\cos\beta - b\sin[\Omega(x+t)]\sin\beta\,,$$

with unknowns amplitude b and phase β. Knowing two values of the numerically computed $u^-(x,t)$ at two different locations x with fixed time t, b and β can be resolved. After the wave is reflected from the impedance boundary, the wave amplitude change is b/a and the wave phase change is $\alpha + \beta$. Hence the reflection coefficient becomes $\hat{W}(\Omega) = \frac{b}{a}\exp[i(\alpha+\beta)]$. The impedance $Z(\Omega)$ is computed from $Z(\Omega) = \frac{1-\hat{W}(\Omega)}{1+\hat{W}(\Omega)}$.

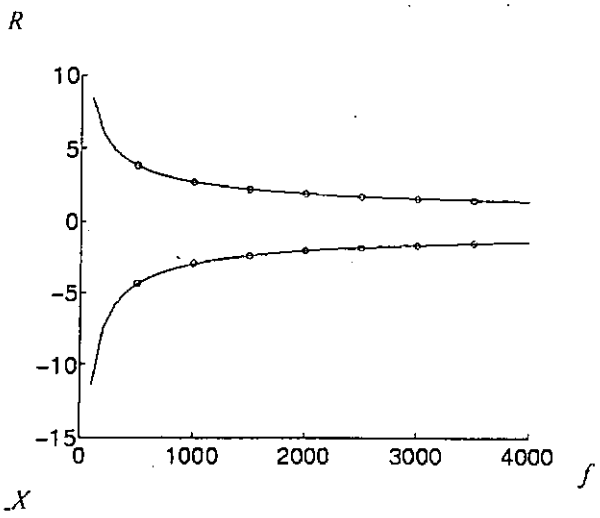

Fig. 3.6. Comparison of the impedance spectrum between the numerically (circle) extracted impedance values with the theoretically (solid line) predicted impedance values. Two-parameter impedance model is embraced.

Fig. 3.6 shows the comparison between the impedance values extracted from the numerical solution (circle) with the theoretical impedance values (solid line) for a material characterized by the two-parameter impedance model.[15] The two-parameter impedance model has the form

$$Z(f) = 0.436(1+i)\sqrt{\frac{\sigma}{f}} + 19.48i\frac{\alpha}{f},\ \sigma = 38000\ Pa\ s\ m^{-2},\ \alpha = 15\ m^{-1},$$

where f is the frequency in Hertz, values of $Z(f)$ are non-dimensional. Eight points per wavelength are necessary in resolving the waves numerically. The results agree well with each other.

Chapter 4 Acoustics Bounded by One Impedance Plane

4.1 Reflection of Harmonic Sources at a Uniform Impedance Plane

The time-domain three-parameter impedance model implemented in the C3N numerical scheme in Chapter 2 has the Fourier transformed frequency-domain equivalence

$$Z(\omega)=R_0+iX_0 =R_0+i(X_{-1}/\omega+X_1\omega), \tag{4.1}$$

where ω is the circular frequency measured in kilo-radian per second, X_{-1} has the same unit as ω, X_1 has the inverse unit as ω. The corresponding time-domain reflection coefficient derived in Chapter 2 has the expression

$$W(t)=\frac{1}{2\pi}\int_{-\infty}^{\infty}\frac{2\dfrac{\omega}{X_1}}{i(\omega-\omega_1)(\omega-\omega_2)}\exp(i\omega t)d\omega-\delta(t),$$

where

$$\omega_{1,2}=\pm\omega_R+i\omega_I,$$

$$\omega_R=\sqrt{\frac{-X_{-1}}{X_1}-\left(\frac{1+R_0}{2X_1}\right)^2}, \tag{4.2a}$$

$$\omega_I=\frac{1+R_0}{2X_1}. \tag{4.2b}$$

For a harmonic sound source with the single frequency Ω, X_{-1} and X_1 may be varied in Eq. (4.1) without the change of the reactance X_0 for the prescribed frequency. Suppose X_1 is taken to be a free parameter, then from Eq. (4.1)

$$X_{-1}=X_0\Omega-X_1\Omega^2. \tag{4.3}$$

To make ω_R real, X_1 in Eq. (4.2a) is being chosen under the constraint

$$X_1\geq X_{1\min}=\frac{1}{2\Omega}\left[X_0+\sqrt{(1+R_0)^2+X_0^2}\right]. \tag{4.4}$$

By suitably picking values of R_0, X_{-1} and X_1 that satisfy Eq. (4.3) and Eq. (4.4), the impedance model in Eq. (4.1) can represent any other impedance model which has the same resistance R_0 and the same reactance X_0 at the prescribed frequency Ω. Fig. 4.1 shows the comparison of the pressure distribution of a harmonic wave reflected from the impedance wall with two different sets of X_{-1} and X_1 values. For demonstration purposes, they are chosen to be $R_0 = 0.2$, $X_{-1} = -13.48$, $X_1 = 0.0739$ (solid line) and $R_0 = 0.2$, $X_{-1} = -14.46696$, $X_1 = 0.1739$ (dashed line) at $f = 500Hz$. X_{-1} and X_1 are dimensional quantities.

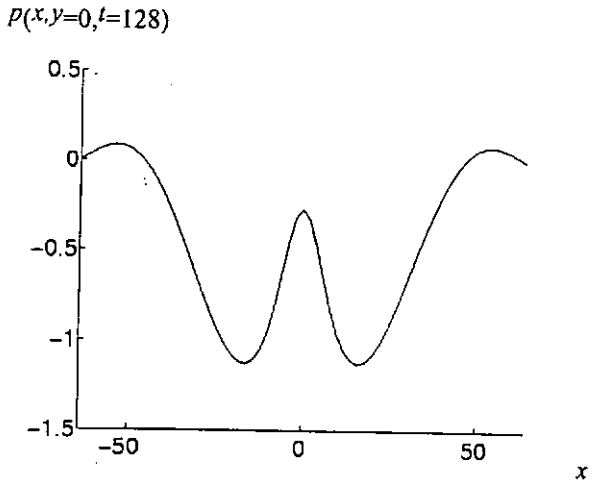

Fig. 4.1. The figure shows the indistinguishable predictions of sound prediction by imposing two different sets of values of X_{-1} and X_1 in Eq. (4.1). $R_0 = 0.2$, $X_{-1} = -13.48$, $X_1 = 0.0739$ (solid line). $R_0 = 0.2$, $X_{-1} = -14.46696$, $X_1 = 0.1739$ (dashed line). Frequency $f = 500$ Hz.

Non-dimensional computational domain is $x \in [-64,64]$ and $y \in [-32,64]$. Acoustic wave is propagating up to the non-dimensional time $t = 128$. The impedance wall is located at $y = -32$. Although sets of values of X_{-1} and X_1 are different, the dimensionless reactance X_0 in Eq. (4.1) remains the same. The plot indicates that there is no discrepancy in the prediction of reflection wave using different sets of values of X_{-1} and X_1. This means that no matter what relationships the sound absorbing materials have, impedance model Eq.

(4.1) could be used provided that the wave is propagating at a single frequency Ω. This concept will be demonstrated by implementing the time-domain equivalent of Eq. (4.1) in the C3N scheme to predict sound reflection from the ground characterized by the two-parameter impedance model proposed by Attenbourough.[16] The two-parameter impedance model has the form

$$Z(\omega) = 0.436(1+i)\sqrt{\frac{76\pi}{\omega}} + 19.48i\left(\frac{0.03\pi}{\omega}\right),$$

where ω is measured in kilo-radian per second. The distributed harmonic source S associated with the numerical computation in Eq. (2.1) will have the form

$$f_x = f_y = 0,$$

$$f_\rho(r_s,t) = \exp\left(-br_s^2\right)\sin(\Omega t)\,,\ r_s = \sqrt{(x-x_s)^2+(y-y_s)^2}\,.$$

(x_s,y_s) is the center of the cylindrical harmonic source, $b = \ln(2)/\gamma^2$ is a constant for the propagation of the sound source, γ is a chosen constant for the wave according to the propagation frequency Ω. This parameter γ is of no significance for far field concerns as long as there are fine enough grid resolution to resolve the pulse $f_\rho(r_s,t)$, and the circular region centered at (x_s,y_s) with radius γ^2 does not overlap with the boundaries. After adjusting the numerical pressure values by the factor $\frac{\pi\Omega}{4b}\exp\left(-\frac{\Omega^2}{4b}\right)$, the results are compared with the zeroth order Hankel function distribution, where the zeroth order Hankel function is the 2-D Green's function for the singular point source. The asymptotic pressure form for the zeroth order Hankel function has the expression

$$p(x,y,t) = -i\Omega\left[\sqrt{\frac{2}{\pi kR_1}}\exp(ikR_1) - Q\sqrt{\frac{2}{\pi kR_2}}\exp(ikR_2)\right]\exp(-i\Omega t)\,, \qquad (4.5)$$

where $k=\Omega/c$ is the wave number, $\Omega=2\pi f$ is the circular frequency of the single frequency wave. Eq. (4.5) may be deduced from the 2-D Weyl Van der Pol formula described in Appendix B.

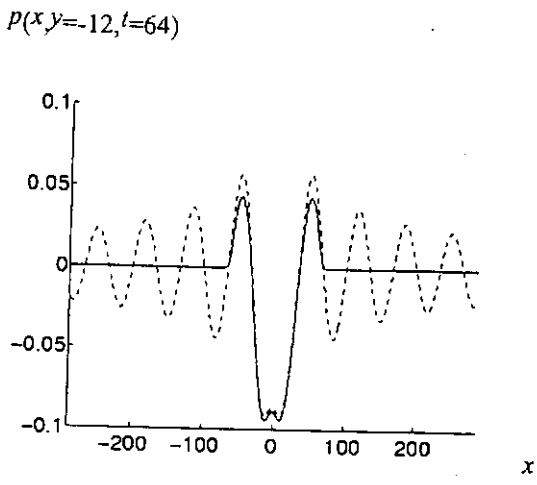

Fig. 4.2 a

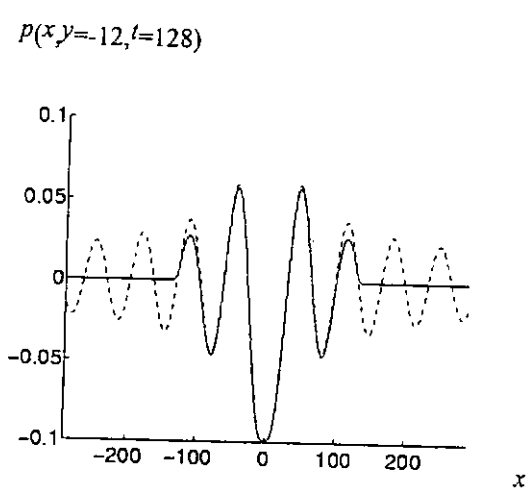

Fig. 4.2 b

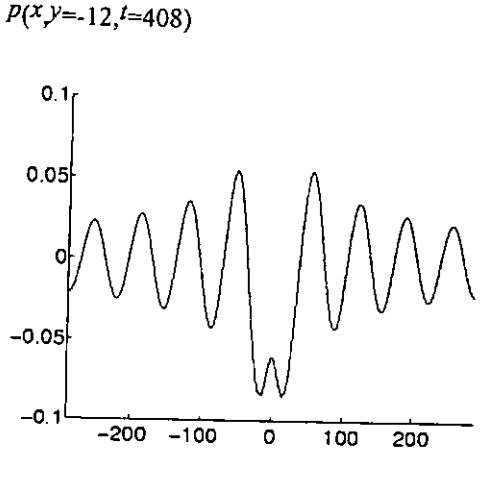

Fig. 4.2 c

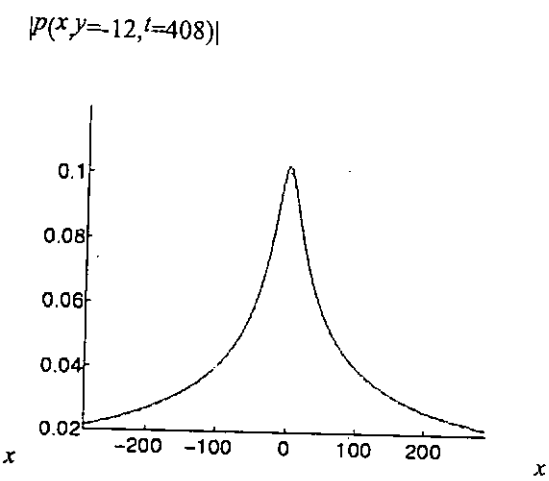

Fig. 4.2 d

Fig. 4.2. The figures are comparisons between the C3N scheme (solid line) and the results predicted by Eq. (4.5) (dashed line). Frequency $f = 500\ Hz$. Source height $h_s = 0.16^m$. Receiver height $h_r = 0.04^m$. Two-parameter impedance model is adopted.

Fig. 4.2 compare the results between the sound pressure level distribution p of the numerical solutions and the solutions obtained from Eq. (4.5) at frequency $f = 500\ Hz$.

Solid line is the 2-D numerical solution. Dashed line is the solution obtained from Eq. (4.5). The sound source is placed at the coordinate system center (0,0). The receiver location is at (x=100,y=-12). The impedance ground is leveled at (x,y =-16). Spatial variable x is the separation distance in the computational domain. Negative values of x means the receiver is to the left of the source. Positive values of x means the receiver is to the right of the source.The coordinate system is non-dimensionlized by the characteristic length $L = 0.01m$ and the characteristic velocity $c = 340m/s$. This corresponds to the physical configuration of source height $h_s = 0.16m$ and receiver height $h_r = 0.04m$.

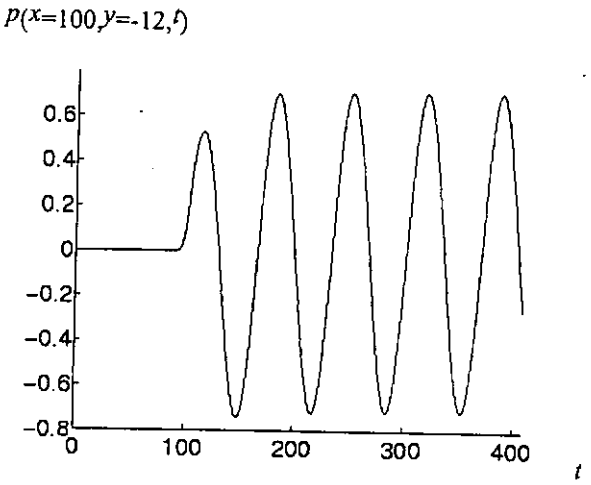

Fig. 4.3. Time history of the pressure variation at a fixed location. Frequency $f = 500\ Hz$. Source height $h_s = 0.16m$. Receiver height $h_r = 0.04m$. Separation distance $r = 1m$.

Fig. 4.3 pictures the time history of the sound pressure level at the receiver location (x=100,y=-12) with the source location at (x=0,y=0). The impedance ground is at (x,y=-16). This corresponds to source height $h_s = 0.16m$, receiver height $h_r = 0.04m$ and separation distance $r = 1m$. Frequency $f = 500\ Hz$. Sound pressure level tends to sinusoidal wave form after about three wavelengths of the propagating wave. The sinusoidal wave form after three wavelengths has sound pressure level with constant amplitude at all time.

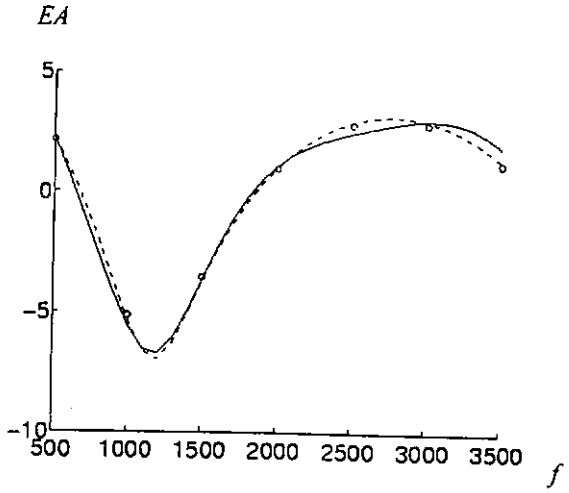

Fig. 4.4. EA predicted by C3N scheme (circles), the boundary element method (solid line) and Eq. (4.5) (dashed line). Source height $h_s = 0.16m$. Receiver height $h_r = 0.3m$. Separation distance $r = 1m$. Two-parameter impedance model is used.

Fig. 4.4 compares the excess attenuation (EA) spectra predicted by the C3N scheme (circle), the boundary element method (BEM) (solid line) and the results of Eq. (4.5) (dashed line). Excess attenuation (EA) is defined as $EA = 20\log_{10}\left|\frac{p_t}{p_d}\right|$. The configuration at all frequencies are the same, source height $h_s = 0.16m$, receiver height $h_r = 0.3m$ and separation distance $r = 1m$. The corresponding non-dimensional source position is at (x=0,y=0), the non-dimensional receiver position is at (x=100,y=14), the impedance boundary is located at (x,y=-16) in the numerical configuration. Results agree fairly well with each other.

4.2 Comparisons with Models for Mixed Impedance Planes

Acoustic pressure estimated by mixed impedance models over a single impedance discontinuity will be compared with the numerical predictions. The models included are the De Jong model and the modified Fresnel-zone models. The De Jong model is built

upon the approximation of the diffraction theory at a semi-infinite wedge. The configuration of the model for various path lengths is depicted in Fig. 4.5.

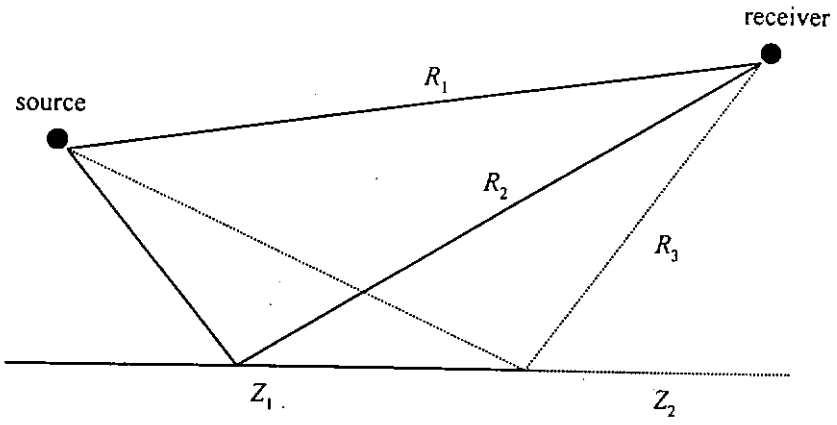

Fig. 4.5. R_1 is the direct path length. R_2 is the reflected path length. R_3 is the path length that passes through the point of impedance discontinuity. Z_1 and Z_2 are the impedance values for the hard and soft ground respectively.

The definition of the excess attenuation (EA) defined by De Jong is

$$EA = 20\log\left|\frac{P}{P_1}\right|,$$

$$\frac{P}{P_1} = 1 + \frac{R_1}{R_2}Q_{1,2}\exp\{ik(R_2 - R_1)\} + \frac{(Q_2 - Q_1)}{\sqrt{\pi}}\frac{R_1}{R_3}\exp\left(-i\frac{\pi}{4}\right)\{F_{31} \pm F_{32}\exp\{ik(R_2 - R_1)\}\},$$

$$F_{31} = F\left(\sqrt{k(R_3 - R_1)}\right), \qquad F_{32} = F\left(\sqrt{k(R_3 - R_2)}\right),$$

$$F(x) = \int_x^\infty \exp(iw^2)dw,$$

where k is the wave number, P is the total wave pressure, P_1 is the direct wave pressure, R_1 is the direct path length from source to receiver, R_2 is reflected path length through the specular reflection point, R_3 is the path length through the impedance discontinuity, Q_1 is the spherical wave reflection coefficient chosen when the specular reflection point falls

on the ground with impedance Z_1, and Q_2 is the spherical wave reflection coefficient chosen when the specular reflection point falls on the ground with impedance Z_2. The plus sign before F_{32} is selected when Q_1 is used. The minus sign before F_{32} is selected when Q_2 is used. $F(x)$ is the Fresnel integral function which can be alternatively expressed as[33]

$$F(x)=\sqrt{\frac{\pi}{2}}[g(x)+if(x)]\exp(ix^2),$$

$$f(x)=\left[\frac{1}{2}-S(x)\right]\cos(x^2)-\left[\frac{1}{2}-C(x)\right]\sin(x^2),$$

$$g(x)=\left[\frac{1}{2}-S(x)\right]\sin(x^2)+\left[\frac{1}{2}-C(x)\right]\cos(x^2),$$

$$C(x)+iS(x)=\frac{1+i}{2}erf\left[\frac{(1-i)x}{2}\right],$$

$$erf(z)=\frac{2}{\sqrt{\pi}}\sum_{n=0}^{\infty}(-1)^n\frac{z^{2n+1}}{n!(2n+1)}.$$

For $|z| \to \infty$ and $|\arg(z)| < 3\pi/4$, the error function is expanded as[34]

$$erf(z)=1-\frac{\exp(-z^2)}{\sqrt{\pi}z}\left[1+\sum_{n=1}^{\infty}(-1)^n\frac{(1)(3)\cdots(2n-1)}{(2z^2)^n}\right]$$

$$=1-\frac{\exp(-z^2)}{\sqrt{\pi}z}\left[1+\sum_{n=1}^{\infty}\prod_{k=1}^{n}\left(-\frac{2k-1}{2z^2}\right)\right].$$

The next mixed impedance models considered are the modified Fresnel-zone models. To evaluate the proportions of impedance of each type contributing to the excess attenuation (EA) at the receiver, Slutsky and Bertoni[30] suggested the use of Fresnel diffraction theory. This theory is further developed into the modified Fresnel-zone models and applied by Hothersall and Harriott.[31] The Fresnel-zone defined in the modified Fresnel-zone models

sweeps out an elliptical area that has the following configuration in the x-y-z coordinate system.

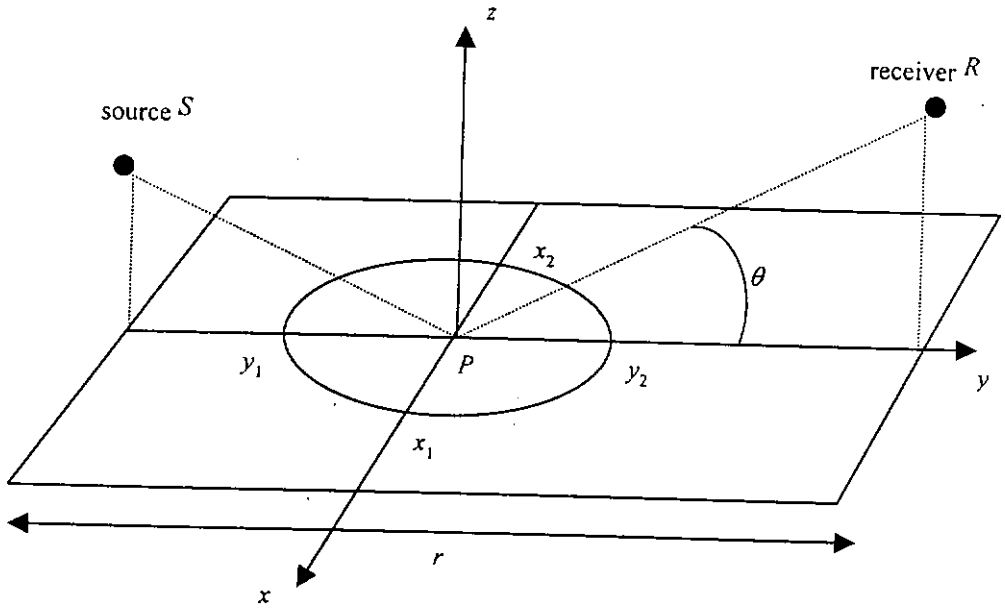

Fig. 4.6. Configuration for the Fresnel-zone model. The elliptical Fresnel zone cuts across the x-axis at $x_{1,2}$ and the y-axis at $y_{1,2}$, θ is the angle of incidence, r is the horizontal separation distance between the source S and the receiver R, point P is the specular reflection point.

The boundary of the Fresnel-zone on the x-y plane is an ellipse which is given by

$$\frac{x^2}{b^2}+\frac{(y\cos\theta-c)^2}{a^2}+\frac{y^2\sin^2\theta}{b^2}=1,$$

$$a=\frac{R_2+F\lambda}{2}, \qquad b=\sqrt{\frac{R_2F\lambda}{2}+\left(\frac{F\lambda}{2}\right)^2}, \qquad c=\frac{R_2}{2}-SP.$$

where θ is the angle between the line PR and the x-y plane, r is the horizontal separation distance between the source and the receiver, F = 1/3 (Hothersall and Harriott[31]), λ is the wavelength of the propagating wave. In Fig. 4.6,

$$x_{1,2} = \pm b\sqrt{1 - \frac{(y_m \cos\theta - c)^2}{a^2} + \frac{y_m \sin\theta}{b^2}},$$

$$y_{1,2} = -\frac{B}{A} \pm \sqrt{\frac{1}{A} - \left(\frac{c\sin\theta}{Aab}\right)^2},$$

$$y_m = \frac{B}{A}, \qquad A = \left(\frac{\cos\theta}{a}\right)^2 + \left(\frac{\sin\theta}{b}\right)^2, \qquad B = \frac{c\cos\theta}{a^2},$$

where $x_{1,2}$ and $y_{1,2}$ are the boundary points of the elliptical Fresnel zone. The first modified Fresnel-zone model in this study was suggested by Hothersall and Harriott. Following their assumption, the excess attenuation (EA) at the receiver is evaluated from

$$EA = \mu 20\log\left|1 + \frac{R_1}{R_2} Q_1 \exp\{ik(R_2 - R_1)\}\right| + (1-\mu)20\log\left|1 + \frac{R_1}{R_2} Q_2 \exp\{ik(R_2 - R_1)\}\right|,$$

where k is the wave number, R_1 is the direct path length, R_2 is the specular reflection path length, Q_1 is the spherical wave reflection coefficient of the ground with impedance Z_1, Q_2 is the spherical wave reflection coefficient of the ground with impedance Z_2, μ is the proportion of the line representing the Fresnel zone that intersects with the area of impedance Z_1, and (1-μ) is the proportion of the line representing the Fresnel zone that intersects with the area of impedance Z_2. The line representing the Fresnel zone is defined as the intersection between the elliptical Fresnel zone and the vertical plane containing source, receiver and specular reflection point. The above EA expression is the linear interpolation of the EA's over the two different impedance grounds. Alternatively, if the pressures over the two different impedance grounds are linearly interpolated instead, a new definition of the excess attenuation is obtained,

$$EA = 20\log\left\{\mu\left|1 + \frac{R_1}{R_2} Q_1 \exp\{ik(R_2 - R_1)\}\right| + (1-\mu)\left|1 + \frac{R_1}{R_2} Q_2 \exp\{ik(R_2 - R_1)\}\right|\right\}.$$

This is termed as the second modified Fresnel-zone model. C3N numerical scheme described in Chapter 2 is capable of solving the wave equation with an arbitrarily prescribed impedance value at each boundary point. Therefore, the scheme is well-adapted for implementing any mixed impedance boundary condition.

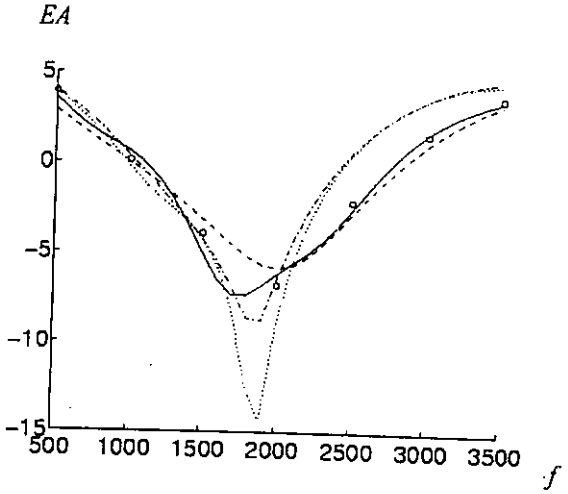

Fig. 4.7. EA spectra comparison. C3N numerical solution (circles). Boundary element method (solid line). De Jong model (dashed line). First modified Fresnel-zone model (dotted line). Second modified Fresnel-zone model (dashed-dot line). Source height h_s=0.16m. Receiver height h_r=0.3m. Separation distance r=1m. The impedance discontinuity is located at r=0.5m. From source to the impedance discontinuity is the hard ground. From impedance discontinuity to the receiver is the impedance ground. Two-parameter impedance model is employed for the impedance ground.

Fig. 4.7 shows the comparisons of the excess attenuation (EA) spectra among the C3N numerical solution, the boundary element method (BEM) and the mixed impedance models. The impedance discontinuity is located half way between the source and the receiver. That is 50% hard ground from source to impedance discontinuity and 50% impedance ground from impedance discontinuity to the receiver. The impedance model employed is the two-parameter impedance model

$$Z(f) = 0.436(1+i)\sqrt{\frac{\sigma}{f}} + 19.48i\frac{\alpha}{f}\ ,\ \sigma = 38000\ Pa\ s\ m^{-2},\ \alpha = 15\ m^{-1}.$$

Frequency f is measured in Hertz (Hz). The configuration in the numerical computation is non-dimensionalized by the characteristic length $L = 0.01m$ and the characteristic velocity c = 340m/s. Fig. 4.7 has the source location at (x=0,y=0) and the receiver location at (x=100,y=14). The impedance boundary is situated at (x,y=-16), x is the horizontal separation distance between the source and the receiver in the numerical configuration. Note that the excess attenuation (EA) defined in the mixed impedance models is different from the definition given by Hothersall and Harriott[32] by a negative sign. Although only single impedance discontinuity phenomenon is presented in this chapter, there are also acoustic grounds with periodic impedance. Grounds with multiple impedance discontinuities are of practical interests. For instance, at outdoor sound propagation, people are interested in adjusting the mixed impedance ground in order to position the first dip of the EA spectra at certain frequencies. The objective is to control the noise level at those particular frequencies. A conjecture on the average sound energy dissipation inside a room with mixed impedance walls is critical in the design of good room acoustics. Such issues are discussed further in Chapter 5.

Pao Yue-Kong Library
PolyU • Hong Kong

Chapter 5 Applications and Extensions

5.1 Overview on Room Acoustics

One of the many important applications of sound prediction methods is on room acoustics. In architectural acoustics, people are always concerned about the echoes inside a building. Too much reflection of sound from the wall will degrade the quality of musical sound during a performance. Since the time of Sabin, criteria for designing a room with good acoustics for specified purposes have been developed extensively. Reverberation time T_{60} computed from the Sabin-Franklin-Jaeger theory plays the central role in the quantitative formulation of some of the simpler criteria.[1] The reverberation time T_{60} is defined as the time required to have the spatial average of the running time average of the acoustic energy inside a room to drop by a factor of 10^6 (60dB). If the reverberation time is too short, the perception of sound inside the room may become undetectable because the loudness of sound is directly proportional to the acoustic energy. If the reverberation time is too long, the information of sound becomes inaudible and the perception decreases even though the sound intensity continues to increase further. Thus, for a given size of a room and a given intensity of a sound source, there is an optimum reverberation time for the room. Experiences show that the optimum reverberation time for a given room volume should be higher for music reception than for speech reception.[1] Experiments have been performed to determine this optimum reverberation time T_{60} by changing the wall coverings with different sound absorbing powers inside a room.

5.2 *Sabin-Franklin-Jaeger Theory*

The theoretical development in obtaining the reverberation time T_{60} is based on the Sabin-Franklin-Jaeger theroy. To derive the theory, one starts from the Euler equations

$$\frac{\partial \rho}{\partial t} + \nabla \cdot \left(\rho \bar{U}\right) = 0, \tag{5.1}$$

$$\rho \frac{\partial \bar{u}}{\partial t} = -\nabla p. \tag{5.2}$$

ρ is the density of air, $\bar{U} = (u, v, w)^T$ is the acoustic velocity vector, ∇ is the del operator, p is the sound pressure level. Subtituting $\rho = \rho_0 + \rho'$, $\bar{U} = (u_0 + u', v_0 + v', w_0 + w')^T$, $p = p_0 + p'$ into Eq. (5.1) to Eq. (5.2) and retaining only the first order terms, we obtain

$$\frac{\partial \rho'}{\partial t} + \nabla \cdot \left(\rho_0 \bar{U}'\right) = 0, \tag{5.3}$$

$$\rho_0 \frac{\partial \bar{U}'}{\partial t} = -\nabla p', \tag{5.4}$$

where ρ_0, p_0 and $\bar{U}_0 = (u_0, v_0, w_0)^T = \bar{0}$ are the ambient density of air, ambient pressure and ambient velocity vector respectively of an undisturbed stage. The primed variables ρ', p' and $\bar{U}' = (u', v', w')$ are the disturbed quantities from the ambient state of the density of air, pressure and velocity vector respectively when there is sound propagation in the flow field. Taking the dot product of $\bar{U}'$ with Eq. (5.4), we obtain

$$\bar{U}' \cdot \left(\rho_0 \frac{\partial \bar{U}'}{\partial t} \right) = -\bar{U}' \cdot \nabla p',$$

or

$$\frac{\rho_0}{2} \frac{\partial \left(\bar{U}' \cdot \bar{U}'\right)}{\partial t} = -\nabla \cdot \left(p' \bar{U}'\right) + p' \nabla \cdot \bar{U}'. \tag{5.5}$$

By substituting Eq.(5.3) into Eq.(5.5) and writing $U'^2 = \bar{U}'\cdot\bar{U}' = u'^2 + v'^2 + w'^2$, we obtain

$$\frac{\rho_0}{2}\frac{\partial U'^2}{\partial t} = -\nabla\cdot\left(p'\bar{U}'\right) - \frac{p'}{\rho_0}\frac{\partial \rho'}{\partial t}. \tag{5.6}$$

If the relation $p = p(\rho)$ is presumed for compressible fluid, then

$$p = p_0 + \left(\frac{\partial p}{\partial \rho}\right)_0 \rho' + \frac{1}{2}\left(\frac{\partial^2 p}{\partial \rho^2}\right)_0 \rho'^2 + \cdots. \tag{5.7}$$

By retaining terms up to the first order together with the definition $\left(\frac{\partial p}{\partial \rho}\right)_0 = c^2$, where c is the sound speed in air, Eq. (5.7) becomes $\rho' = \frac{p'}{c^2}$. Substituting this relation into Eq. (5.6) and taking away the prime (') sign, we obtain

$$\frac{\partial E}{\partial t} + \nabla\cdot\bar{I} = 0, \tag{5.8}$$

where $E = \frac{1}{2}\rho_0 U^2 + \frac{1}{2}\frac{p^2}{\rho_0 c^2}$ is known as the acoustic energy which is the sum of the acoustic kinetic energy and the acoustic potential energy respectively, $\bar{I} = p\bar{U}$ is known as the acoustic energy flux or the acoustic intensity. Eq. (5.8) is the energy conservation law of acoustics expressed in differential form. If E and $\bar{I}$ are replaced by the running time averages $\overline{E}$ and $\overline{\bar{I}}$ respectively, Eq. (5.8) still holds true. To prove this, it is known that for each frequency of the spherical waves interacting inside a room, the acoustic potential is just the superposition of waves with wave form $A(r,\theta)\exp[i(r-ct)]$. $|A(r,\theta)|$ is the amplitude of a wave which is inversely proportional to the radial distance r, r is the radial distance from the source to the receiver if the wave is a direct wave or r is the radial distance from the image source to the receiver if the wave is a reflected wave.

Hence the corresponding velocity U and pressure p would have the wave forms $U = A_U(r,\theta)\exp[i(r-ct)]$ and $p = A_p(r,\theta)\exp[i(r-ct)]$ respectively. Putting these forms into Eq. (5.8) and taking the running time average, we have

$$\frac{1}{T}\int_{t'}^{t'+T}\left[\frac{1}{2}\frac{\partial}{\partial t}\left(\rho_0 A_U^2\exp[2i(r-ct)]+\frac{1}{\rho_0 c^2}A_p^2\exp[2i(r-ct)]\right)+\nabla\cdot\bar{I}\right]dt=0,$$

where T is the integral number of a half wave period, t' is any time instance which is itself an independent time variable. Thus, from the above equation,

$$\frac{1}{T}\int_{t'}^{t'+T}\left[-ic\left(\rho_0 A_U^2\exp[2i(r-ct)]+\frac{1}{\rho_0 c^2}A_p^2\exp[2i(r-ct)]\right)+\nabla\cdot\bar{I}\right]dt=0,$$

or

$$\frac{\partial\bar{E}}{\partial t'}+\nabla\cdot\bar{\bar{I}}=0.$$

The second term on the left of the above equation is not immediately obvious from its previous equation. But it can be proved by mathematical analysis. However, the proof is omitted in the present context. By replacing t' by t, we have the running time average acoustic energy of conservation law

$$\frac{\partial\bar{E}}{\partial t}+\nabla\cdot\bar{\bar{I}}=0, \tag{5.9}$$

where $\bar{E}$ is the running time average acoustic energy and is defined as

$$\bar{E}=\frac{1}{4}\rho_0|A_U|^2+\frac{1}{4}\frac{|A_p|^2}{\rho_0 c^2}.$$

By definition, the running time average acoustic energy is the average of the minimum and the maximum amplitudes of the squared sinusoidal quantity, which is precisely what

$\overline{E}$ is. For a squared sinusoidal quantity $f = A^2 \sin^2 t$ say, the running time average of f can be determined as

$$\bar{f} = \frac{1}{T}\int_s^{s+T} f dt = \frac{1}{T}\int_s^{s+T} |A|^2 \sin^2 t dt = \frac{|A|^2}{2T}\int_s^{s+T} [1-\cos(2t)]dt = \frac{|A|^2}{2T}\left[t - \frac{1}{2}\sin(2t)\right]_s^{s+T} = \frac{|A|^2}{2},$$

where T is the integral number of the half wave period of f. This indicates that the running time average of f is just the average of the minimum amplitude of f (= 0) and the maximum amplitude of f (= $|A|^2$). To express Eq. (5.9) in integral form, one needs to integrate this equation over an arbitrarily chosen volume V. As a result,

$$\iiint_V \frac{\partial \overline{E}}{\partial t} dV + \oiint_S \overline{\vec{I}} \cdot \vec{n} dS = 0. \tag{5.10}$$

Eq. (5.10) is the running time average conservation law of acoustic energy for an empty room. S is the surface enclosing the volume V, $\vec{n}$ is the unit normal vector pointing outward of the volume V. Now consider the first term on the left of Eq. (5.10),

$$\iiint_V \frac{\partial \overline{E}}{\partial t} dV = \frac{\partial}{\partial t}\left(\lim_{\Delta V \to 0} \sum_n \overline{E}_n \Delta V\right)$$

$$= \frac{\partial}{\partial t}\left(\lim_{\substack{\Delta V \to 0 \\ N \to \infty}} \frac{\sum_n \overline{E}_n}{N} N\Delta V\right)$$

$$= \frac{\partial \overline{\overline{E}}}{\partial t} V.$$

$\overline{\overline{E}}$ is the spatial average of the running time average of the acoustic energy, $\overline{E}_n$ is the value of $\overline{E}$ in each of the corresponding infinitesimally small volume ΔV. The surface integral on the left of Eq. (5.10) is drawn from the Gauss theorem and is known as the

acoustic power. This acoustic power includes the power emitted from the sound source and the power lost due to the sound energy absorbed by and/or transmitted through the walls. If we denote P as the acoustic power of the sound source, P_d as the acoustic power dissipated at the wall, then Eq. (5.10) becomes

$$V\frac{\partial \overline{\overline{E}}}{\partial t} = \overline{\overline{P}} - \overline{\overline{P_d}}. \tag{5.11}$$

The double bar over each of the quantity denotes the spatial average of the running time average of the corresponding quantity. From the statistical assumptions,[1] $\overline{\overline{P_d}}$ is dependent on $\overline{\overline{E}}$ and room properties with the expression $\overline{\overline{P_d}} = \frac{c}{4}\left(\sum_i \alpha_i A_i\right)\overline{\overline{E}}$, α_i is the absorption coefficient of the wall covering with area A_i. It has the expression $\alpha_i = (1-Q_i)(1+Q_i)$ and Q_i is the spherical wave reflection coefficient of the corresponding wall covering material, c is the sound speed in air. Substituting $\overline{\overline{P_d}} = \frac{c}{4}\left(\sum_i \alpha_i A_i\right)\overline{\overline{E}}$ into Eq. (5.11), we obtain

$$V\frac{\partial \overline{\overline{E}}}{\partial t} + \frac{c}{4}\left(\sum_i \alpha_i A_i\right)\overline{\overline{E}} = \overline{\overline{P}}.$$

After the waves have made a hundredth reflections from the wall, the source power is turned off (i.e. $\overline{\overline{P}} = 0$ at $t = 0$). The solution of the above differential equation becomes,

$$\overline{\overline{E}}(t) = \overline{\overline{E_0}}\exp\left(-\frac{t}{\tau}\right), \qquad \tau = \frac{4V}{c\sum_i \alpha_i A_i}, \tag{5.12}$$

where $\overline{\overline{E_0}}$ is the spatial average of the running time average of the acoustic energy at the instance when the source is turned off. The reverberation time T_{60} is the time when

$\frac{\bar{\bar{E}}}{\bar{\bar{E}}_0} = 10^{-6}$. Putting $t = T_{60}$ into Eq. (5.12), we have $T_{60} = (6\ln 10)\tau$. This expression is the Sabin-Franklin-Jaeger theory for the reverberation time T_{60}.

5.3 *Acoustic Field with Stratified Fluid, Mean Velocity or Entropy Variations*

There are many extensions of the time-domain approach beyond the frequency-domain approach in the prediction of sound fields. For example, the density of air could vary with height at the outdoor sound propagation. A wind current might be blowing over an acoustic field. Acoustic propagation in air might have an entropy change. For fluid with entropy change, heat transfer and viscosity become factors in the sound propagation. More precisely, acoustic pressure will depend on both fluid density and entropy. Henceforth, the governing equations of acoustics with entropy change will be the mass conservation equation, the momentum transport equations and the energy transport equation. All of the situations mentioned above cannot be easily dealt with by the frequency-domain approach. Therefore, the time-domain numerical approach is a general approach to cope with all the realistic situations.

Chapter 6 Closing Remarks and Suggested Future Work

Time-domain impedance boundary condition has been derived for the three-parameter frequency-domain impedance model. Numerical results using this time-domain impedance boundary condition agree well with the frequency-domain prediction of sound pressure level.

The Laplace transform method has been applied to the one-dimensional piston problem with impedance boundary condition. The resulting series is a divergent series that is not uniformly valid for all time. However, by truncating the divergent series to a finite series, it approximates the true solution with accuracy dependent on the number of terms in the finite series.

The demonstration of using the three-parameter time-domain impedance model to predict sound fields reflected from a material characterized by the two-parameter frequency-domain impedance model is successful. This shows that by implementing a fixed impedance model in the C3N scheme, the numerical code can surmise sound fields reflected from any other surface with a different impedance model provided that the sound wave is traveling at a single frequency.

For the suggested future work, the time-domain numerical predictions on acoustic problems with broadband frequencies sound source should be attempted. Sound propagation problems predicted by the C3N scheme with fluid density stratification, mean flow or entropy variation should further be investigated.

References

[1]Alan D. Pierce "Acoustics: an introduction to its physical principles and applications" McGraw Hill book Co. p107-108, 1981.

[2]Keith Attenborough, "Review of ground effects on outdoor sound propagation from continuous broadband sources," Applied Acoustics 24 (1988) 289-319.

[3]Volker Mellert, Christian Nocke and Sabine Teuber, "Surface impedance measurement with spherical wave reflection coefficient for inhomogeneous samples," Procceedings of Inter-Noise 95, p1093-1096, 1995 July 10-12.

[4]A. J. Cramond and C. G. Don, "Reflection of impulses as a method of determining acoustic impedance," J. Acoust. Soc. Am. 75 (2), 382-389, February 1984.

[5]C. F. Don abd A. J. Cramond, "Soil impedance measurements by an acoustic pulse technique," J. Acoust. Soc. Am. 77 (4), 1601-1609, April 1985.

[6]G. A. Daigle and Michael R. Stinson, "Impedance of grass-covered ground at low frequencies measured using a phase difference technique," J. Acoust. Soc. Am. 81 (1), 62-68, January 1987.

[7]J. C. Davies and K. A. Mulholland, "An impulse method of measuring normal impedance at oblique incidence," Journal of Sound and Vibration (1979) 67(1), 135-149.

[8]Michael G. Jones and Patricai E. Stiede, "Comparison of methods for determining specific acoustic impedance," J. Acoust. Soc. Am. 101(5), Pt. 1, 2694-2704, May 1997.

[9]C. Nocke, V. Mellert, T. Waters-Fuller, K. Attenborough and K. M. Li, "Impedance deduction from broad-band, point-source measurements at grazing incidence," ACUSTICA (acta acustica), vol. 83 (1997) 1085-1090.

[10]Leonid M. Brekhovskikh, "Waves in layered media," Academic press, p239, 1960.

[11]C. F. Chien and W. W. Soroka, "Sound propagation along an impedance plane," Journal of Sound and Vibration (1975) 43(1), 9-20.

[12]C. F. Chien and W. W. Soroka, "A note on the calculation of sound propagation along an impedance surface," Journal of Sound and Vibration (1980) 69(2), 340-343.

[13]Keith Attenborough, "Ground parameter information for propagation modeling," J. Acoust. Soc. Am. 92(1), 418-427, July 1992.

[14]T. F. W. Embleton, J. E. Piercy and N. Olson, "Outdoor sound propagation over ground of finite impedance," J. Acoust. Soc. Am., vol 59, No. 2, 267-277, February 1976.

[15]Kai Ming Li, Shahram Taherzadeh and Keith Attenborough, "Sound propagation from a dipole source near an impedance plane, " J. Acoust. Soc. Am. 101 (6), 3343-3352, June 1997.

[16]K. Y. Fung and Bhanuprakash Tallapragada, "Time-domain impedance boundary condition for waves," Proceedings of Noise-Con 97, p103-108, June 15-17 1997.

[17]Christopher K. W. Tam and Laurent Auriault, "Time-domain impedance boundary conditions for computational aeroacoustics," AIAA Jouranl vol. 34, N0. 5, 917-923, May 1996.

[18]Christian Y. Glandier, Carole E. Floc'h and Mohamed A. Hamdi, "Analytical, numerical and experimental study of the acoustic behavior of a rectangular cavity with absorbing treatment on a wall," AIAA Journal 1997, 747-754.

[19]Victor W. Sparrow, "Lattice gas methods for computational aeroacoustics," Second computational aeroacoustics workshop on benchmark problems, November 1996.

[20]Cheolwan Kim and Philip Roe, "Acoustic calculations with second- and fourth-order upwind leapfrog schemes, " Second computational aeroacoustics workshop on benchmark problems, November 1996.

[21]John W. Goodrich, "Application of a new finite difference algorithm for computational aeroacoustics, " ICASE/LaRC workshop on benchmark problems in computational aeroacoustics, Oct. 1994.

[22]Lei Tang and James D. Baeder, "The construction of high-accuracy schemes for acoustic equations," ICASE/LaRC workshop on benchmark problems in computational aeroacoustics, Oct. 1994.

[23]C. K. W. Tam and J. C. Webb, "Dispersion-relation-preserving difference schemes for computational acoustics," Journal of Computational Physics, vol. 107, No. 2, 1993, 262-281.

[24]Mark H. Carpenter, David Gottlieb and Saul Abarbanel, "Stable and accurate boundary treatments for compact, high-order finite-difference schemes, " Applied numerical mathematics 12 (1993) 55-87.

[25]Mark H. Carpenter, David Gottlieb and Saul Abarbanel, "Time-stable boundary conditions for finit-difference schemes solving hyperbolic systems : methodology and application to high-order compact schemes," Journal of computational physics 111, 220-236 (1994).

[26]K. Y. Fung, Raymond S. O. Man and Sanford Davis, "Implicit high-order compact algorithm for computational acoustics," AIAA Journal vol. 34, No. 10, October 1996, 2029-2037.

[27]Patrice Boulanger, Tim Waters-Fuller, Keith Attenborough and Kai Ming Li, "Models and measurements of sound propagation from a point source over mixed impedance ground," J. Acoust. Soc. Am. 102 (3), 1432-1442, September 1997.

[28]D. Botteldooren, "Acoustical finite-difference time-domain simulation in a quasi-Cartesian grid", J. Acoust. Soc. Am. 95(5), Pt. 1, 2313-2319, May 1994.

[29]D. Botteldooren, "Finite-difference time-domain simulation of low-frequency room acoustic problems", J. Acoust. Soc. Am. 98(6), 3302-3308, December 1995.

[30]S. Slustky and H. L. Bertoni, "Analysis and programs for assessment of absorptive and tilted parallel barriers," Transportation Research Record 1176, Transportation Research Record, National Research Council, Washington, DC. 13-22 (1987).

[31]D. C. Hothersall and J. N. B. Harriott, "A Fresnel zone approach to the prediction of sound propagation above a multi-impedance plane," Proc. Inst. Acoust. 16, 83-90 (1994).

[32]D. C. Hothersall and J. N. B. Harriott, "Approximate models for sound propagation above multi-impedance plane boundaries", J. Acoust. Soc. Am. 97(2), 918-926, February 1995.

[33]Nico M. Temme, "Special Functions – An introduction to the classical functions of mathematical physics", New York, Wiley, 1996.

[34]S. Zhang and J. Jin, "Computation of special functions", New York, John Wiley, 1996.

Appendix A Derivation of the Weyl Van der Pol Formula

Sound pressure level predicted by the Weyl Van der Pol formula has been applied successfully to sound wave reflected from a soft wall. The Weyl Van der Pol formula is the solution of the 3-D acoustic wave problem with impedance boundary condition. The theory assumes a pulse as the sound source. The expression $\delta(x)\delta(y)\delta(z\text{-}h_s)\delta(t\text{-}0^+)$ is a mathematical function which corresponds to a physical pulse starts at position $(0,0,h_s)$ and at time $t = 0^+$, δ is the Dirac delta function and h_s is the source height. Sound wave propagation in time-domain is modeled by the wave equation. On the plane $z = 0$, the impedance boundary condition is imposed. In all the other directions, free boundary conditions or the Sommerfeld radiation condition at infinity are described. The mathematical problem that accounts all of the above statements may be formulated as

$$\phi_{tt} - c^2(\phi_{xx} + \phi_{yy} + \phi_{zz}) = 0, \quad -\infty < x < \infty, \quad -\infty < y < \infty, \quad z > 0, \quad t > 0, \tag{A.1a}$$

$$\phi(x, y, z, 0) = 0, \tag{A.1b}$$

$$\phi_t(x, y, z, 0^+) = c^2\delta(x)\delta(y)\delta(z - h_s)\delta(t - 0^+), \tag{A.1c}$$

$$-ik\hat{\phi}(x, y, 0, k) = Z\hat{\phi}_z(x, y, 0, k), \tag{A.1d}$$

$$\lim_{x\to\pm\infty} \phi(x, y, z, t) = \lim_{y\to\pm\infty} \phi(x, y, z, t) = \lim_{z\to+\infty} \phi(x, y, z, t) = 0. \tag{A.1e}$$

Now define a temporal integral transform on ϕ as

$$\hat{\phi} = \int_0^\infty \phi \exp(-ikct)dt\,. \tag{A.2}$$

Define a two-folded Fourier transform in x and y as

$$\tilde{\phi} = \int_{-\infty}^{\infty}\int_{-\infty}^{\infty} \hat{\phi} \exp\left[-i(k_x x + k_y y)\right]dxdy\,. \tag{A.3}$$

By applying the transforms of Eq. (A.2) and (A.3) to Eq. (A.1), we obtain

$$\tilde{\phi}_{zz} + (k^2 - k_x^2 - k_y^2)\tilde{\phi} = -\delta(z - h_s), \tag{A.4a}$$

$$-ik\tilde{\phi}(k_x,k_y,0,k) = Z\tilde{\phi}_z(k_x,k_y,0,k), \tag{A.4b}$$

$$\lim_{z\to+\infty}\tilde{\phi}(k_x,k_y,z,k) = 0. \tag{A.4c}$$

Define a transform in z by

$$\bar{\phi} = \int_0^\infty \tilde{\phi}\exp(-ik_z z)dz.$$

Applying the above transform to Eq. (A.4), we obtain

$$(k^2 - k_x^2 - k_y^2 - k_z^2)\bar{\phi} = -\exp(-ik_z h_s) + i(k_z - k\beta)\tilde{\phi}(k_x,k_y,0,k),$$

where $\beta = 1/Z$ is the admittance of the acoustic surface. Hence

$$\bar{\phi}(k_x,k_y,k_z,k) = \frac{-\exp(-ik_z h_s) + i(k_z - k\beta)\tilde{\phi}(k_x,k_y,0,k)}{k^2 - k_x^2 - k_y^2 - k_z^2}. \tag{A.5}$$

Define an inverse Fourier transform in z as,

$$\tilde{\phi} = \frac{1}{2\pi}\int_{-\infty}^{\infty}\bar{\phi}\exp(ik_z z)dk_z.$$

Applying the above transform to Eq. (A.5), we obtain

$$\tilde{\phi}(k_x,k_y,z,k) = -\frac{i}{2k_z}\left[-\exp(ik_z\mid z-h_s\mid) + i(k_z - k\beta)\tilde{\phi}(k_x,k_y,0,k)\exp(ik_z z)\right], \tag{A.6}$$

where

$$k_z = \sqrt{k^2 - k_x^2 - k_y^2}.$$

Substituting $z = 0$ into Eq. (A.6), we obtain

$$\tilde{\phi}(k_x,k_y,0,k) = \frac{i\exp(ik_z h_s)}{k_z + k\beta}.$$

Hence Eq. (A.6) becomes,

$$\tilde{\phi}(k_x,k_y,z,k) = \frac{i}{2k_z}\left[\exp(ik_z\mid z-h_s\mid) + \left(1 - \frac{2k\beta}{k_z + k\beta}\right)\exp(ik_z(z+h_s))\right]. \tag{A.7}$$

Define a two-folded inverse Fourier transform in k_x and k_y as

$$\hat{\phi} = \frac{1}{4\pi^2} \int_{-\infty}^{\infty}\int_{-\infty}^{\infty} \tilde{\phi} \exp\left[i(k_x x + k_y y)\right] dk_x dk_y \,.$$

Applying the above transform to Eq. (A.7), we obtain

$$\hat{\phi}(x,y,z,k) = \frac{i}{8\pi^2} \int_{-\infty}^{\infty}\int_{-\infty}^{\infty} \frac{\exp(ik_z \mid z - h_s \mid)}{k_z} dk_x dk_y$$

$$+ \frac{i}{8\pi^2} \int_{-\infty}^{\infty}\int_{-\infty}^{\infty} \frac{\exp(ik_z (z + h_s))}{k_z} dk_x dk_y$$

$$+ \frac{i}{8\pi^2} \int_{-\infty}^{\infty}\int_{-\infty}^{\infty} - \frac{2k\beta}{k_z (k_z + k\beta)} \exp(ik_z (z + h_s)) dk_x dk_y \qquad \text{(A.8)}$$

The first integral on the right is the direct wave term that has been evaluated by Brekhovskikh.[10] The second integral on the right is the reflected wave term that can be evaluated by residue theorem from complex analysis. The third integral on the right corresponds to the surface wave term which is evaluated by Chien and Soroka.[11,12] The result of Eq. (A.8) is

$$\phi \cong \frac{\exp(ikR_1)}{4\pi R_1} + Q \frac{\exp(ikR_2)}{4\pi R_2}, \qquad \text{(A.9a)}$$

$$Q = R(\theta) + (1 - R(\theta)) F(p_e), \qquad \text{(A.9b)}$$

$$R(\theta) = \frac{\cos(\theta) - \beta}{\cos(\theta) + \beta}, \qquad \text{(A.9c)}$$

$$F(p_e) = 1 + i\sqrt{\pi}\, p_e \exp(-p_e^2) erfc(-ip_e), \qquad \text{(A.9d)}$$

$$p_e = \sqrt{\frac{1}{2} ikR_2}\,[\beta + \cos(\theta)]. \qquad \text{(A.9e)}$$

The above equation is known as the Weyl Van der Pol formula. The symbol (^) on ϕ indicates the frequency-domain solution is eliminated for clarity. Time dependence of exp(-$i\omega t$) is assumed. The geometry and the notations of the theoretical derivation are indicated in Fig. A.1.

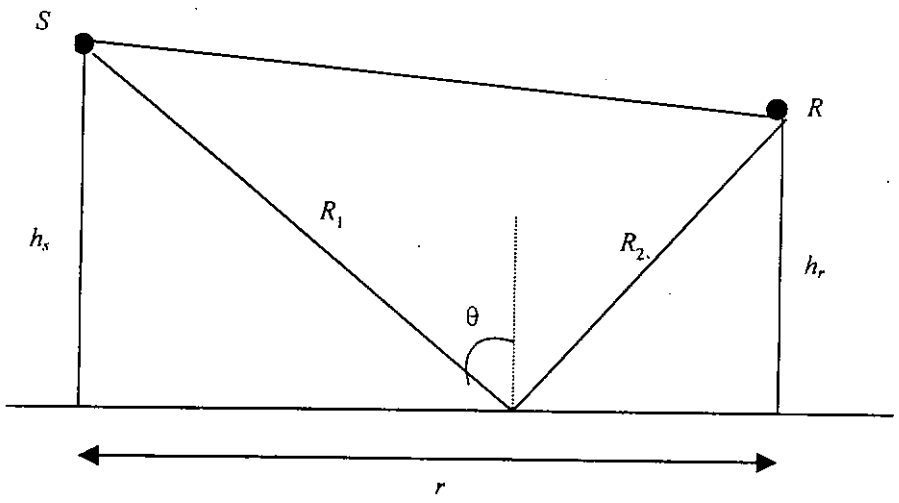

Fig. A.1. Geometry used in theory and experiment. S denotes the position of the source at height h_s, R is the position of receiver at height h_r, r is the separation distance between the source and the receiver, R_1 is the path length of the direct wave, R_2 is the path length of the specularly reflected wave, θ is the angle of incidence from the normal axis.

If the receiver R is located at position (x,y,z) and the source S is at $(0,0,h_s)$, then

$$R_1 = \sqrt{x^2 + y^2 + (z - h_s)^2},$$

$$R_2 = \sqrt{x^2 + y^2 + (z + h_s)^2}.$$

Appendix B Construction of the 2-D Weyl Van der Pol Formula

The Weyl Van der Pol formula is designed as a solution of the 3-D wave problem. Sometimes a 2-D wave problem is being studied for theoretical importance. A 2-D sound wave has the zeroth order Hankel function distribution. If the spherical wave reflection coefficient is assumed in the 2-D reflection from an impedance wall, then the solution is the same as Eq. (A.9) except Eq. (A.9a) may be replaced by

$$\phi \cong H_0(kR_1) + QH_0(kR_2). \tag{B.1}$$

$H_0(.)$ is the zeroth order Hankel function. Eq. (B.1) and Eq. (A.9b) to Eq. (A.9e) is termed as the 2-D Weyl Van der Pol formula. The evaluation of the spherical wave reflection coefficient Q in Eq. (A.9) involves the complementary error function $erfc(-ip_e)$. A complete description on the evaluation of this complementary error function $erfc(ip_e)$ is mentioned in Chien and Soroka.[12] The details are repeated below.

Define

$$w(z) = \exp(-z^2)erfc(-iz),$$

where $z = x + iy$. If $x > 6$ or $y > 6$,

$$w(z) = iz\left(\frac{0.5124242}{z^2 - 0.2752551} + \frac{0.05176536}{z^2 - 2.724745}\right) + \eta(z),$$

$|\eta(z)| < 10^{-6}$. If $x > 3.9$ or $y > 3$,

$$w(z) = iz\left(\frac{0.4613135}{z^2 - 0.1901635} + \frac{0.09999216}{z^2 - 1.7844927} + \frac{0.002883894}{z^2 - 5.5253437}\right) + \varepsilon(z),$$

$|\varepsilon(z)| < 2 \times 10^{-6}$. If $x < 0$ or $y < 0$,

$$w(-x + iy) = \overline{w(x + iy)},$$

$$w(x - iy) = 2\exp(y^2 - x^2)[\cos(2xy) + i\sin(2xy)] - \overline{w(x + iy)}.$$

For smaller absolute values of x and y,

$$erf(-iz) = \frac{2}{\sqrt{\pi}} \sum_{n=0}^{\infty} \frac{(-1)^n (-iz)^{2n+1}}{n!(2n+1)},$$

$$erfc(-iz) = 1 - erf(-iz),$$

$$w(z) = \exp(-z^2) erfc(-iz).$$

A sample "C" program for the evaluation of the 2-D Weyl Van der Pol formula of Eq. (B.1) and Eq. (A.9b) to Eq. (A.9e) is included as follows.

```
/*####################
Header file "complex.h"
####################*/

typedef struct complex complex;

complex Czero();
complex Cone();
complex CA(complex,complex);
complex CS(complex,complex);
complex CM(complex,complex);
complex CD(complex,complex);
complex CC(complex);
complex Cexp (complex);

#include "sub.h"

struct complex
{
 double real;
 double imag;
}

/*################
Header file "sub.h"
################*/

complex erf1 (complex);
complex erf2 (complex);
complex erf3 (complex);
complex erfcc (complex);
complex Hankel0 (double);
complex weyl (double,double,double,double,double);

/*##############################################
Subroutine "fmain.c". This returns the excess attenuation.
##############################################*/
```

```
#include <stdio.h>
#include <math.h>
#include "complex.h"

main ()
{
 double f, t, hs, hr, r, df, dfh, fmin, fmax, L, EA;
 complex K;

 L = 0.01;
 hs = 16.0*L;
 hr = 4.0*L;
 r = 100.0*L;
 t = 256.0*L/340.0;

 df = 100.0;
 dfh = df/2.0;
 fmin = 500.0;
 fmax = 20000.0+dfh;

 for (f=fmin;f<fmax;f=f+df)
 {
  K = weyl(f,hs,hr,r,t);
  EA = sqrt(K.real*K.real+K.imag*K.imag);
  EA = 20.0*log10(EA);

  printf ("%lf\n", EA);
 }
}
```

```
#include "complex.c"

/*####################
Subroutine "complex.c"
####################*/

complex Czero ()
{
 complex zero;

 zero.real = 0.0;
 zero.imag = 0.0;

 return zero;
}

complex Cone ()
{
 complex one;
```

```
  one.real = 1.0;
  one.imag = 0.0;

  return one;
 }

 complex CA (a,b)
 complex a, b;
 {
  complex c;

  c.real = a.real+b.real;
  c.imag = a.imag+b.imag;

  return c;
 }

 complex CS (a,b)
 complex a, b;
 {
  complex c;

  c.real = a.real-b.real;
  c.imag = a.imag-b.imag;

  return c;
 }

 complex CM (a,b)
 complex a, b;
 {
  complex c;

  c.real = a.real*b.real-a.imag*b.imag;
  c.imag = a.real*b.imag+a.imag*b.real;

  return c;
 }

 complex CD (a,b)
 complex a, b;
 {
  complex c;
  double temp;

  temp = b.real*b.real+b.imag*b.imag;
  c.real = (a.real*b.real+a.imag*b.imag)/temp;
  c.imag = (-a.real*b.imag+a.imag*b.real)/temp;
```

```
  return c;
 }

 complex CC (a)
 complex a;
 {
  complex c;

  c.real = a.real;
  c.imag = -a.imag;

  return c;
 }

 complex Cexp (a)
 complex a;
 {
  double temp;
  complex c;

  temp = exp(a.real);
  c.real = temp*cos(a.imag);
  c.imag = temp*sin(a.imag);

  return c;
 }

 #include "sub.c"

 /*################
 Subroutine "sub.c"
 ################*/

 #include "erf1.c"
 #include "erf2.c"
 #include "erf3.c"
 #include "erfcc.c"
 #include "Hankel0.c"
 #include "weyl.c"

 /*################
 Subroutine "erf1.c"
 ################*/

 complex erf1 (pe)
 complex pe;
 {
  complex w, z, z2, zz, a, b, k;

  z = pe;
```

```
  z2 = CM(z,z);

  zz.real = z.imag*z.imag-z.real*z.real;
  zz.imag = 2.0*z.real*z.imag;
  w = Czero();

  a.real = 0.5124242;
  a.imag = 0.0;
  b.real = 0.2752551;
  b.imag = 0.0;
  w = CA(w,CD(a,CS(z2,b)));

  a.real = 0.05176536;
  a.imag = 0.0;
  b.real = 2.724745;
  b.imag = 0.0;
  w = CA(w,CD(a,CS(z2,b)));

  k.real = 0.0;
  k.imag = 1.0;

  w = CM(k,CM(z,w));

  if (pe.imag<0.0)
  {
   a.real = 2.0;
   a.imag = 0.0;
   k = CM(a,Cexp(zz));

   if (pe.real>0.0) w = CC(CS(k,w));
   else w = CS(CC(k),w);
  }
  else if (pe.real<0.0) w = CC(w);

  return w;
}

/*###############
Subroutine "erf2.c"
###############*/

complex erf2 (pe)
complex pe;
{
 complex w, z, z2, zz, a, b, k;

 z = pe;
 z2 = CM(z,z);

 zz.real = z.imag*z.imag-z.real*z.real;
```

```
  zz.imag = 2.0*z.real*z.imag;
  w = Czero();

  a.real = 0.4613135;
  a.imag = 0.0;
  b.real = 0.1901635;
  b.imag = 0.0;
  w = CA(w,CD(a,CS(z2,b)));

  a.real = 0.09999216;
  a.imag = 0.0;
  b.real = 1.7844927;
  b.imag = 0.0;
  w = CA(w,CD(a,CS(z2,b)));

  a.real = 0.002883894;
  a.imag = 0.0;
  b.real = 5.5253437;
  b.imag = 0.0;
  w = CA(w,CD(a,CS(z2,b)));

  k.real = 0.0;
  k.imag = 1.0;

  w = CM(k,CM(z,w));

  if (pe.imag<0.0)
  {
   a.real = 2.0;
   a.imag = 0.0;
   k = CM(a,Cexp(zz));

   if (pe.real>0.0) w = CC(CS(k,w));
   else w = CS(CC(k),w);
  }
  else if (pe.real<0.0) w = CC(w);

  return w;
}

/*###############
Subroutine "erf3.c"
###############*/

complex erf3 (pe)
complex pe;
{
 int n, NumTerm;
 double pi, factn;
 complex z, z2, pe2, kw, K, k, w;
```

```
  pi = 3.14156265359;
  NumTerm = 100;

  K.real = 0.0;
  K.imag = -1.0;

  z = CM(K,pe);
  z2 = CM(z,z);
  pe2 = CM(pe,pe);
  k = z;
  w = z;

  factn = 1.0;
  for (n=1;n<=NumTerm;n++)
  {
   k = CM(k,z2);
   factn = factn*n;

   K.real = factn*(2.0*n+1.0);
   K.imag = 0.0;
   if ((n%2) != 0) K.real = -K.real;

   w = CA(w,CD(k,K));
  }

  K.real = 2.0/sqrt(pi);
  K.imag = 0.0;

  w = CS(Cone(),CM(K,w));
  w = CM(Cexp(CS(Czero(),pe2)),w);

  return w;
}

/*################
Subroutine "erfcc.c"
################*/

complex erfcc (pe)
complex pe;
{
 double x, y;
 complex w;

 x = fabs(pe.real);
 y = fabs(pe.imag);

 if ((x>6.0) || (y>6.0)) w = erf1 (pe);
 else if ((x>3.9) || (y>3.0)) w = erf2 (pe);
```

```
  else w = erf3 (pe);

  return w;
}

/*#########################################################################
Subroutine "Hankel0.c". This returns asymptotic form of the zeroth-order
Hankel function.
#########################################################################*/

complex Hankel0 (z)
double z;
{
 double pi, J, Y, k;
 complex H;

 pi = 3.14156265359;
 k = pi/4.0;

 J = sqrt(2/pi/z)*cos(z-k);
 Y = sqrt(2/pi/z)*sin(z-k);

 H.real = J;
 H.imag = Y;

 return H;
}

/*#########################################################################
Subroutine "weyl.c". This returns the ratio of the total SPL to the direct SPL.
#########################################################################*/

complex weyl (f,hs,hr,r,t)
double f,hs,hr,r,t;
{
 double R1, R2, k, wt;
 double pi, theta, omega, temp;
 complex K, cosT, dexpiwt;
 complex Z, W, beta, pe, R, F, w;
 complex phi, direct, reflect;

 pi = 3.14156265359;
 k = 2.0*pi*f/340.0;

 R1 = sqrt((hr-hs)*(hr-hs)+r*r);
 R2 = sqrt((hr+hs)*(hr+hs)+r*r);

 theta = atan(r/(hs+hr));

 Z.real = 0.436*sqrt(38000.0/f);
```

```
  Z.imag = Z.real+19.48*15.0/f;

  beta = CD(Cone(),Z);

  cosT.real = cos(theta);
  cosT.imag = 0.0;

  R = CD(CS(cosT,beta),CA(cosT,beta));

  K.real = sqrt(k*R2)/2.0;
  K.imag = K.real;
  pe = CM(K,CA(cosT,beta));

  w = erfcc(pe);

  K.real = 0.0;
  K.imag = sqrt(pi);
  F = CA(Cone(),CM(K,CM(pe,w)));

  W = CA(R,CM(CS(Cone(),R),F));

  omega = k*340.0;
  wt = omega*t;

  direct = Hankel0(k*R1);
  reflect = Hankel0(k*R2);

  dexpiwt.real = k*0.01*sin(wt);
  dexpiwt.imag = k*0.01*cos(wt);

  phi = CA(direct,CM(W,reflect));
/*
  phi = CM(phi,dexpiwt);
*/
  return CD(phi,direct);
}
```